bioRxiv preprint doi: https://doi.org/10.1101/2021.03.13.435281; this version posted March 14, 2021. The copyright holder for this preprint (which was not certified by peer review) is the author/funder. All rights reserved. No reuse allowed without permission.

Updating the steady state model of C_4 photosynthesis

Susanne von Caemmerer

Australian Research Council Centre of Excellence for Translational Photosynthesis, Division of Plant Sciences, Research School of Biology, The Australian National University, Acton, ACT 2601, Australia

Email: Susanne.caemmerer@anu.edu.au

Running title: Steady state model of C_4 photosynthesis

bioRxiv preprint doi: https://doi.org/10.1101/2021.03.13.435281; this version posted March 14, 2021. The copyright holder for this preprint (which was not certified by peer review) is the author/funder. All rights reserved. No reuse allowed without permission.

Highlight

The C_4 photosynthesis model by von Caemmerer and Furbank (1999) has been updated. It now includes temperature dependencies and equations to calculate electron transport rate from measured CO_2 assimilation rates.

Abstract

C_4 plants play a key role in world agriculture. For example, C_4 crops such as maize and sorghum are major contributors to both first and third world food production and the C_4 grasses sugarcane; miscanthus and switchgrass are major plant sources of bioenergy. In the challenge to manipulate and enhance C_4 photosynthesis, steady state models of leaf photosynthesis provide and important tool for gas exchange analysis and thought experiments that can explore photosynthetic pathway changes. Here the C_4 photosynthetic model by von Caemmerer and Furbank (1999) has been updated with new kinetic parameterisation and temperature dependencies added. The parameterisation was derived from experiments on the C_4 monocot, *Setaria viridis*, which for the first time provides a cohesive parametrisation. Mesophyll conductance and its temperature dependence have also been included, as this is an important step in the quantitative correlation between the initial slope of the CO_2 response curve of CO_2 assimilation and in vitro PEP carboxylase activity. Furthermore, the equations for chloroplast electron transport have been updated to include cyclic electron transport flow and equations have been added to calculate electron transport rate from measured CO_2 assimilation rates.

Key words:

A-ci curves, C_4 photosynthesis, chloroplast electron transport, CO_2 diffusion, leaf temperature, PEP carboxylase

bioRxiv preprint doi: https://doi.org/10.1101/2021.03.13.435281; this version posted March 14, 2021. The copyright holder for this preprint (which was not certified by peer review) is the author/funder. All rights reserved. No reuse allowed without permission.

Introduction

To meet the challenge of increasing crop yield for a growing world population, it has become apparent that photosynthetic efficiency and capacity must be increased per unit leaf area to improve yield potential (Long *et al.*, 2015). High yields from C_4 crops have stimulated considerable interest in the C_4 photosynthetic pathway which is characterised by high photosynthetic rate and high nitrogen and water use efficiency relative to plants with the C_3 photosynthetic pathway (Mitchell and Sheehy, 2006). In the challenge to increase photosynthetic rate per leaf area steady state models of leaf photosynthesis provide an important tool for gas exchange analysis and thought experiments that can explore photosynthetic pathway changes (Long *et al.*, 2015; Price *et al.*, 2011; von Caemmerer and Evans, 2010; von Caemmerer and Furbank, 2016; von Caemmerer *et al.*, 2003). The mathematical simplicity of these leaf level models has facilitated incorporation into higher order canopy, crop and earth system models (Rogers *et al.*, 2017; Wu *et al.*, 2018; Wu *et al.*, 2019; Yin and Struik, 2009).

C_4 photosynthesis requires the coordinated functioning of mesophyll and bundle-sheath cells of leaves and is characterised by a CO_2 concentrating mechanism which allows Rubisco, located in the bundle sheath cells, to operate at high CO_2 partial pressures. This overcomes the low affinity Rubisco has for CO_2 and largely inhibits its oxygenation reaction, reducing photorespiration rates. In the mesophyll, CO_2 is initially fixed by phosphoenolpyruvate (PEP) carboxylase into C_4 acids, which are then decarboxylated in the bundle sheath to supply CO_2 for Rubisco. Both the structure of the bundle-sheath wall (which has a low permeability to CO_2) and the relative biochemical capacities of the C_3 cycle in the bundle sheath and C_4 acid cycle (which operates across the mesophyll bundle-sheath interface) contribute to the high CO_2 partial pressure in the bundle sheath. The biochemistry of the C_4 photosynthetic pathway is not unique and three main biochemical subtypes are recognised on a basis of the predominant decarboxylating enzyme: NADP-ME (NADP-dependent malic enzyme), NAD-ME (NAD-dependent malic enzyme) and PEPCK (PEP carboxykinase) (Hatch, 1987).

The first models to capture the C_4 photosynthetic biochemistry were designed by Berry and Farquhar (1978) and (Peisker, 1979). The Berry and Farquhar model did not provide analytical solutions but was able to predict high bundles sheath CO_2 partial pressures and its dependence on bundle sheath conductance. Many of the gas exchange characteristics of C_4

bioRxiv preprint doi: https://doi.org/10.1101/2021.03.13.435281; this version posted March 14, 2021. The copyright holder for this preprint (which was not certified by peer review) is the author/funder. All rights reserved. No reuse allowed without permission.

photosynthesis observed with intact leaves could be predicted by these models. Collatz *et al*. (1992) and von Caemmerer and Furbank (1999) have revised and expanded these original models with analytical solutions.

C_4 models have not been used as frequently as the C_3 models so less data relating leaf biochemistry with gas exchange is available in the literature. Massad *et al*. (2007) have parameterised the model by von Caemmerer (2000) for *Zea mays* and developed the first temperature dependencies for key parameters. Fitting routines have also been developed (Bellasio *et al.*, 2016; Bellasio *et al.*, 2017; Zhou *et al.*, 2019).

Here an update of the C_4 photosynthetic model by von Caemmerer and Furbank (1999) and von Caemmerer (2000) is provided with new parameterisation and temperature dependencies derived from experiments on the C_4 monocot species *Setaria viridis* (green foxtail millet), a NADP-malic enzyme type which is closely related to agronomically important C_4 crops. It has become a popular model species due to its rapid generation time, small stature, high seed production, diploid status and small sequenced and publicly available genome and it can be readily transformed (Alonso-Cantabrana *et al.*, 2018; Brutnell *et al.*, 2010; Doust, 2007; Ermakova *et al.*, 2019; Li and Brutnell, 2011; Osborn *et al.*, 2016).

The basic model equations

Figure 1 shows a schematic representation of the proposed carbon fluxes in C_4 photosynthesis. After diffusion of CO_2 across the mesophyll cell interface CO_2 is converted to HCO_3^- by carbonic anhydrase, CA, which is fixed by PEP carboxylase, PEPC into C_4 acids, which diffuse to and are decarboxylated in the bundle sheath. Rubisco and the complete C_3 photosynthetic pathway are located in the bundle-sheath cells, bounded by a relatively gas tight cell wall such that the C_3 cycle relies almost entirely on C_4 acid decarboxylation as its source of CO_2.

The net rate of CO_2 fixation for C_4 photosynthesis can be given by two equations. The first describes Rubisco carboxylation in the bundle sheath. Since all carbon fixed into sugars ultimately must be fixed by Rubisco, overall CO_2 assimilation, A, can be given by

bioRxiv preprint doi: https://doi.org/10.1101/2021.03.13.435281; this version posted March 14, 2021. The copyright holder for this preprint (which was not certified by peer review) is the author/funder. All rights reserved. No reuse allowed without permission.

$$A = V_c - 0.5V_o - R_d \quad (1)$$

where V_c and V_o are the rates of Rubisco carboxylation and oxygenation and R_d is the rate of mitochondrial respiration not associated with photorespiration.

Mitochondrial respiration may occur in the mesophyll as well as in the bundle sheath. As Rubisco may more readily refix CO_2 released in the bundle sheath, R_d is described by its mesophyll and bundle-sheath components

$$R_d = R_m + R_s. \quad (2)$$

CO_2 assimilation rate, A, can also be written in terms of the mesophyll reactions as

$$A = V_p - L - R_m, \quad (3)$$

where V_p is the rate of PEP carboxylation, R_m is the mitochondrial respiration occurring in the mesophyll and L is the rate of CO_2 leakage from the bundle sheath to the mesophyll (Figure 1). This assumes that in the steady state the rate of PEP carboxylation and the rate of C_4 acid decarboxylation are equal.

The leak rate, L, is given by

$$L = g_{bs}(C_s - C_m) \quad (4)$$

where g_{bs} is the conductance to CO_2 leakage and is determined by the properties of the bundle-sheath cell wall; C_s and C_m are the bundle sheath and mesophyll CO_2 partial pressures. It is assumed that there is a negligible amount of HCO_3^- leakage from the bundle sheath since the HCO_3^- pool should be small due to the absence of carbonic anhydrase activity in the cytosol of these cells (Farquhar, 1983; Jenkins *et al.*, 1989; Ludwig *et al.*, 1998).

The C_4 cycle consumes additional energy during the regeneration of PEP and leakage of CO_2 from the bundle sheath is an energy cost to the leaf. This represents a compromise between retaining CO_2, allowing efflux of O_2 and permitting metabolites to diffuse in and out at rates fast enough to support the rate of CO_2 fixation (Hatch and Osmond, 1976; Raven, 1977). The CO_2 leak rate depends upon the balance between the rates of PEP carboxylation and Rubisco activity and the conductance of the bundle sheath to CO_2.

bioRxiv preprint doi: https://doi.org/10.1101/2021.03.13.435281; this version posted March 14, 2021. The copyright holder for this preprint (which was not certified by peer review) is the author/funder. All rights reserved. No reuse allowed without permission.

Leakiness (ϕ), a term coined by Farquhar (1983), defines leakage as a fraction of the rate of PEP carboxylation and thus describes the efficiency of the C_4 cycle

$$\phi = L/V_p. \quad (5)$$

A related term "overcycling" has also been used (Furbank *et al.*, 1990; Jenkins, 1989). Overcycling defines the leak rate as a fraction of CO_2 assimilation rate and gives the fraction by which the flux through the C_4 acid cycle has to exceed net CO_2 assimilation rate

$$Overcycling = {}^{L}/_{A} = \left(V_p - (A + R_m)\right)/A. \quad (6)$$

C_4 photosynthesis can be either limited by the enzymatic rates of PEP carboxylase and Rubisco or by the irradiance and the capacity of chloroplast electron transport which supports the regeneration of PEP and RuBP.

Enzyme limited rate equations

Many important features of the C_4-model can be examined with the enzyme-limited rates, which are presumed to be appropriate under conditions of high irradiance. As is the case in C_3 models of photosynthesis (Farquhar and von Caemmerer, 1982; Farquhar *et al.*, 1980; von Caemmerer, 2000), Rubisco carboxylation at high irradiance can be described by its RuBP saturated rate

$$V_c = \frac{C_s V_{cmax}}{C_s + K_c(1 + O_s/K_o)} \quad (7)$$

where O_s is the O_2 partial pressure in the bundle sheath. Following the oxygenation of one mol of RuBP, 0.5 mol of CO_2 is evolved in the photorespiratory pathway and the ratio of oxygenation to carboxylation can be expressed as

$$V_o/V_c = 2\Gamma_*/C_s \quad (8)$$

where Γ_* is the CO_2 compensation point in a C_3 plant in the absence of other mitochondrial respiration, and

$$\Gamma_* = 0.5[V_{omax}K_c/V_{cmax}K_o]O_s = \gamma_* O_s, \quad (9)$$

bioRxiv preprint doi: https://doi.org/10.1101/2021.03.13.435281; this version posted March 14, 2021. The copyright holder for this preprint (which was not certified by peer review) is the author/funder. All rights reserved. No reuse allowed without permission.

where the term in the bracket is the reciprocal of Rubisco specificity, $S_{c/o}$ (Farquhar *et al.*, 1980). In what follows the O_2 dependence of Γ_* is highlighted since the O_2 partial pressure in the bundle sheath may vary.

The Rubisco limited rate of CO_2 assimilation can be derived from equations 1, 7, 8 and 9.

$$A_c = \frac{(C_s - \gamma_* O_s)V_{cmax}}{C_s + K_c(1 + O_s/K_o)} - R_d. \quad (10)$$

To derive an overall expression for CO_2 assimilation rate as a function of mesophyll CO_2 and O_2 partial pressure, C_m and O_m, one needs to derive an expression for C_s and O_s. Equation 10 can be used to derive an expression for C_s:

$$C_s = \frac{\gamma_* O_s + K_c(1 + O_s/K_o)((A + R_d)/V_{cmax})}{1 - (A + R_d)/V_{cmax}}. \quad (11)$$

If V_{cmax} could be estimated accurately from biochemical measurements together with A it would provide a means of estimating bundle sheath CO_2 partial pressure. One can also obtain an expression for C_s from equation 3 and 4:

$$C_s = C_m + \frac{V_p - A - R_m}{g_{bs}}. \quad (12)$$

Photosystem II activity and O_2 evolution in the bundle sheath varies widely amongst the C_4 species. Some NADP-ME species such as *Zea mays* and *Sorghum bicolor* have little or none, whereas NADP -ME dicots and NAD and PCK species can have high PSII activity (Chapman *et al.*, 1980; Hatch, 1987; Pfundel and Pfeffer, 1997). In S. viridis the amount of PSII activity depends on growth light environment (Ermakova *et al.*, 2021). Because the bundle sheath is a fairly gas tight compartment this has implications for the steady state O_2 partial pressure of the bundle sheath (Berry and Farquhar, 1978; Raven, 1977). Following Berry and Farquhar (1978), we assume that the net O_2 evolution, E_o, in the bundle sheath cells equals its leakage, L_o, out of the bundle sheath, that is

$$E_o = L_o = g_o(O_s - O_m). \quad (13)$$

The conductance to leakage of $O_{2=}$ across the bundle sheath, g_o can be related to the conductance to CO_2 by way of the ratio of diffusivities and solubilities by

$$g_o = g_{bs}(D_{O2}S_{O2}/D_{CO2}S_{CO2}), \quad (14)$$

bioRxiv preprint doi: https://doi.org/10.1101/2021.03.13.435281; this version posted March 14, 2021. The copyright holder for this preprint (which was not certified by peer review) is the author/funder. All rights reserved. No reuse allowed without permission.

where D_{O2} and D_{CO2} are the diffusivities for O_2 and CO_2 in water, respectively and S_{O2} and S_{CO2} are the respective Henry constants such that

$$g_o = 0.047 g_{bs} \quad (15)$$

at 25° C (Berry and Farquhar, 1978; Farquhar, 1983). If $E_o=\alpha A$, where α ($0<\alpha>1$) denotes the fraction of O_2 evolution occurring in the bundle sheath, then O_s:

$$O_s = \frac{\alpha A}{0.0047\, g_{bs}} + O_m. \quad (16)$$

Like Berry and Farquhar (1978), it is assumed that a steady state balance exists between the rate of PEP carboxylation and the release of C_4 acids in the bundle sheath. Furthermore, it is assumed that PEP carboxylation provides the rate limiting step and not, for example, the rate of hydration of CO_2 by carbonic anhydrase. As PEP carboxylase utilises HCO_3^- rather than CO_2, hydration of CO_2 is really the first step in carbon fixation in C_4 species (Hatch and Burnell, 1990).

When CO_2 is limiting the rate of PEP carboxylation is given by a Michaelis Menten equation

$$V_p = \frac{C_m V_{pmax}}{C_m + K_p} \quad (17)$$

where V_{pmax} is the maximum PEP carboxylation rate, K_p is the Michaelis Menten constant for CO_2. This assumes that the substrate PEP is saturating under these conditions. When the rate of PEP regeneration is limiting, for example by the capacity of pyruvate orthophosphate dikinase (PPDK) then

$$V_p = V_{pr} \quad (18)$$

where V_{pr} is a constant (Peisker, 1986; Peisker and Henderson, 1992) and

$$V_p = min\left\{\frac{C_m V_{pmax}}{C_m + K_p}, V_{pr}\right\} \quad (19)$$

To obtain an overall rate equation for CO_2 assimilation as a function of the mesophyll CO_2 and O_2 partial pressures (C_m and O_m) one combines equations (10), (12) and (16). The resulting expression is a quadratic of the form

bioRxiv preprint doi: https://doi.org/10.1101/2021.03.13.435281; this version posted March 14, 2021. The copyright holder for this preprint (which was not certified by peer review) is the author/funder. All rights reserved. No reuse allowed without permission.

$$aA_c^2 + bA_c + c = 0, \quad (20)$$

where

$$A_c = \left(-b + \sqrt{b^2 - 4ac}\right)/(2a) \quad (21)$$

$$a = \frac{\alpha}{0.047}\frac{K_c}{K_o} \quad (22)$$

$$b = -\left\{\left(V_p - R_m + g_{bs}C_m\right) + \left(V_{cmax} - R_d\right) + g_{bs}\left(K_c(1 + O_m/K_o)\right) + \frac{\alpha}{0.047}\left(\gamma_* V_{cmax} + R_d\, K_c/K_o\right)\right\} \quad (23)$$

$$c = \left(V_{cmax} - R_d\right)\left(V_p - R_m + g_{bs}C_m\right) - \left(V_{cmax} g_{bs}\gamma_* O_m + R_d g_{bs} K_c(1 + O_m/K_o)\right) \quad (24)$$

Equation (21) can be approximated by:

$$A_c = min\left\{\left(V_{cmax} - R_d\right), \left(V_p - R_m + g_{bs}C_m\right)\right\} \quad (25)$$

where min { } stands for minimum of.

At low CO_2 partial pressures, CO_2 assimilation rate can be approximated by

$$A_c = \frac{C_m V_{pmax}}{C_m + K_p} - R_m + g_{bs}C_m. \quad (26)$$

Under these conditions A_c is linearly related to the maximum PEP carboxylase activity, V_{pmax}. The product $g_{bs}C_m$ is the inward diffusion of CO_2 into the bundle sheath and because g_{bs} is low (0.003 mol m^{-2} s^{-1}) the flux is only 0.3 µmol m^{-2} s^{-1} at C_m of a 100 µbar and can thus be ignored. At high CO_2 partial pressures CO_2 assimilation rate is given by either the maximal Rubisco activity, V_{cmax} or the rate of PEP regeneration (V_{pr}).

Light and electron transport limited rate equations

The energy requirements for the regeneration of RuBP in the bundle sheath are the same as in a C_3 leaf (Farquhar *et al.*, 1980; von Caemmerer, 2000). There is however the additional cost of 2 mol ATP for the regeneration of one mol of PEP from pyruvate in the mesophyll such that:

bioRxiv preprint doi: https://doi.org/10.1101/2021.03.13.435281; this version posted March 14, 2021. The copyright holder for this preprint (which was not certified by peer review) is the author/funder. All rights reserved. No reuse allowed without permission.

219 $$\text{Rate of ATP consumption} = 2V_p + (3 + 7\gamma_* O_s/C_s)V_c \quad (27)$$

220 where $(7\gamma_* O_s/C_s)V_c$ is the energy requirement due to photorespiration (since $V_o/V_c =$
221 $2\gamma_* O_s/C_s$)(Berry and Farquhar, 1978). In the PCK type C_4 species some of the ATP for PEP
222 regeneration may come from the mitochondria such that the photosynthetic requirement
223 may be less (for review see Furbank, 2011).
224 There is no net NADPH requirement by the C_4 cycle itself, although for example in NADP-ME
225 species NADPH consumed in the production of malate from OAA in the mesophyll is released
226 in the bundle sheath during decarboxylation (Hatch and Osmond, 1976). This may have
227 implications on the behaviour of C_4 photosynthesis under fluctuating light environments (Krall
228 and Pearcy, 1993; Kubásek *et al.*, 2013). The rate of NADP consumption is given by the
229 requirement of the C_3 cycle:

230 $$\text{Rate of NADP consumption} = (2 + 4\gamma_* O_s/C_s)V_c. \quad (28)$$

231 It is important to note that under most situations C_s is probably sufficiently large that the
232 photorespiratory term in equations 27 and 28 can be ignored, but it does become relevant at
233 low mesophyll CO_2 partial pressures, or at very low light (Siebke *et al.*, 1997).
234

235 NADPH and ATP are produced by chloroplast electron transport. The reduction of $NADP^+$ to
236 NADPH + H^+ requires the transfer of 2 electrons through the whole chain electron transport
237 which in turn requires 2 photons each at photosystem II (PSII) and Photosystem I (PSI). The
238 generation of ATP can be coupled to the proton production via whole chain electron
239 transport, or ATP can be generated via cyclic electron transport around PSI.

240 Photosystem II activity in the bundle sheath varies amongst C_4 species with different C_4
241 decarboxylation types. Presumably, when PSII is deficient or absent from the bundle sheath
242 chloroplasts, some ATP is generated via cyclic photophosphorylation and 50% of the NADPH
243 required for the reduction of PGA is derived from NADPH generated by $NADP^+$ malic enzyme
244 (Chapman *et al.*, 1980). The remainder of the PGA must be exported to the mesophyll
245 chloroplast where it is reduced and then returned to the bundle sheath (Hatch and Osmond,
246 1976). Measurements of metabolite pools of *Amaranthus edulis,* a NAD^+ malic enzyme
247 species, having PSII activity in the bundle sheath, suggest that it may also export a part of the

bioRxiv preprint doi: https://doi.org/10.1101/2021.03.13.435281; this version posted March 14, 2021. The copyright holder for this preprint (which was not certified by peer review) is the author/funder. All rights reserved. No reuse allowed without permission.

PGA to the mesophyll for reduction (Leegood and von Caemmerer, 1988). It appears therefore that energy production and consumption is shared between mesophyll and bundle sheath cells more generally across decarboxylation types (von Caemmerer and Furbank, 2016).

A very simple approach was taken in the basic photosynthesis model. Electron transport is modelled as a whole, allocating a different fraction of it to the C_4 and C_3 cycle rather than compartmenting it to mesophyll and bundle sheath chloroplasts (von Caemmerer, 2000; von Caemmerer and Furbank, 1999).

That is whole chain linear electron transport

$$J = J_m + J_s \quad (29)$$

and $J_m = xJ$ and $J_s = (1-x)J$ where 0<x>1. Because at most 2 out of 5 ATP are required in the mesophyll, $x \approx 0.4$ (equation 27). This partitioning approach of electron transport has been adopted by subsequent users of the model (Kromdijk *et al.*, 2010; Massad *et al.*, 2007; Ubierna *et al.*, 2011; Yin and Struik, 2009; Yin *et al.*, 2011; Zhou *et al.*, 2017). Peisker (1988) has modelled the optimisation of *x* at low light in some detail. See also Figure 4.22 in von Caemmerer (2000).

New information exists for the calculation of the ATP requirement. Following Furbank et al. (1990), von Caemmerer and Furbank assumed a stoichiometry of 3 H^+ per ATP produced and the operation of a Q-cycle (von Caemmerer, 2000; von Caemmerer and Furbank, 1999) . Current models of rotational catalysis predict that the H^+/ATP ratio is identical to the stoichiometric ratio of c-subunits to β-subunits which is c/β = 4.7 for spinach chloroplasts (Vollmar *et al.*, 2009). However measured values are closer to 4 for the chloroplast enzyme (Petersen *et al.*, 2012). If 4 H^+ are required per ATP generated, it seems necessary to also have a functional Q-cycle which yields 3 H^+ per linear electron flow. The proton production during cyclic electron flow is only 2 H^+ per electron so that the overall proton production per electron is dependent on the balance of linear to cyclic electron flow (Yin and Struik, 2012).

Following the derivations by Yin and Struik (2012), the rate of proton production from linear and cyclic electron flow is

$$J_{H^+} = 3\,J + 2J_{cyc} = \frac{3-f_{cyc}}{1-f_{cyc}}J \quad (30)$$

bioRxiv preprint doi: https://doi.org/10.1101/2021.03.13.435281; this version posted March 14, 2021. The copyright holder for this preprint (which was not certified by peer review) is the author/funder. All rights reserved. No reuse allowed without permission.

Since $J_1 = J + J_{cyc} = J/(1 - f_{cyc})$ where J_1 is the electron flow out of photosystem 1 and f_{cyc} is the fraction of J_1 that precedes via cyclic electron flow. For details see Figure 2. The rate of ATP production is given by

$$J_{ATP} = J_{H^+}/h = \frac{3-f_{cyc}}{h(1-f_{cyc})} J = zJ \quad (31)$$

Where *h* is the number of protons required per ATP generated, which here is assumed to be 4 and *z* relates linear electron flow J to the rate of ATP production (Yin and Struik, 2012). It follows that

$$J_m = \frac{2}{z} V_p \quad (32)$$

Where z=0.75 when there is no cyclic electron flow and z=1.25 when f_{cyc} =0.5.

$$J_s = \frac{3}{z}(1 + 7\gamma_* O_s/3C_s)V_c. \quad (33)$$

The relationship between the electron transport, J, and the absorbed irradiance that is used here is the same as that used previously where

$$\theta J^2 - J(I_2 + J_{max}) + I_2 J_{max} \quad (34)$$

I_2 is the photosynthetically useful light absorbed by PSII, J_{max} is the maximum electron transport and θ is an empirical curvature factor. 0.7 is a good average value for C_3 species (Evans, 1989) but has not been explored for C_4 species. I_2 is related to incident irradiance by

$$I_2 = I * absorptance\,(1 - f)/2 \quad (35)$$

In sunlight the absorptance of leaves is commonly about 0.85 and *f* is to correct for spectral quality of the light (~0.15 (Evans, 1987)). Ögren and Evans (1993) give a detailed discussion of the parameters of equation 16. The 2 in the denominator is because we assume half the light absorbed needs to reach each photosystem. This assumption may need to be considered as with an increase in cyclic electron flow commonly observed in C_4 species less than half of the light may be absorbed by PSII.

bioRxiv preprint doi: https://doi.org/10.1101/2021.03.13.435281; this version posted March 14, 2021. The copyright holder for this preprint (which was not certified by peer review) is the author/funder. All rights reserved. No reuse allowed without permission.

Putting it all together gives a light and electron transport limited quadratic expression. From equations (3) and (1) one can derive two equations for an electron transport limited CO_2 assimilation rate

$$A_j = \frac{z}{2} xJ \quad - g_{bs}(C_s - C_m) - R_m \tag{36}$$

and

$$A_j = \frac{(1-\gamma_* O_s/C_s)\frac{z}{3}(1-x)J}{(1+7\gamma_* O_s/3C_s)} - R_d \tag{37}$$

Equation (37) can be solved for the bundle sheath CO_2 partial pressure and

$$C_s = \frac{(\gamma_* O_s)\left(7/3\left(A_j+R_d\right)+z(1-x)J \quad /3\right)}{z(1-x)J \quad /3-\left(A_j+R_d\right)}. \tag{38}$$

Combining equations (16), (36) and (36) then yields a quadratic expression of the form

$$aA_j^2 + bA_j + c = 0, \tag{39}$$

where

$$A_j = \left(-b + \sqrt{b^2 - 4ac}\right)/(2a) \tag{40}$$

and

$$a = 1 - \frac{7\gamma_* \alpha}{3*0.047} \tag{41}$$

$$b = -\left\{\left(\frac{z}{2} xJ \quad - R_m + g_{bs} C_m\right) + \left(\frac{z}{3}(1-x)J \quad - R_d\right) + g_{bs}\left(\frac{7\gamma_* O_m}{3}\right) + \frac{\alpha\gamma_*}{0.047}\left(\frac{z}{3}(1-x)J \quad + \frac{7}{3} R_d\right)\right\} \tag{42}$$

bioRxiv preprint doi: https://doi.org/10.1101/2021.03.13.435281; this version posted March 14, 2021. The copyright holder for this preprint (which was not certified by peer review) is the author/funder. All rights reserved. No reuse allowed without permission.

317 $$c = \left(\left(\frac{z}{2}xJ \quad - R_m + g_{bs}C_m\right)\left(\frac{z}{3}(1-x)J \quad - R_d\right) - g_{bs}\gamma_* O_m\left(\frac{z}{3}(1-x)J \quad + \frac{7R_d}{3}\right)\right)$$

318 (43)

319 Equation (4.40) can be approximated by

320 $$A_j = min\left\{\left(\frac{z}{2}xJ \quad - R_m + g_{bs}C_m\right), \left(\frac{z}{3}(1-x)J \quad - R_d\right)\right\} \qquad (44)$$

321 Where min { } stands for minimum of. Sometimes, when the equations are used to fit gas
322 exchange measurements it is sufficient to use equation (44).

323 ## Summary of equations

324 Equations (21) and (40) are the two basic equations of the C_4 model and

325 $$A = min\{A_c, A_j\}. \qquad (45)$$

326 Peisker and Henderson (1992) pointed out that either the enzyme activity or the substrate
327 regeneration rate can limit both Rubisco and PEP carboxylase reactions and that in theory
328 four types of combinations of rate limitations are possible. In the way the electron transport
329 limited equations are presented here, it is assumed that light or the electron transport
330 capacity limit both PEP and RuBP regeneration rates simultaneously. In the model of C_3
331 photosynthesis by Farquhar et al. (1980) and von Caemmerer and Farquhar (1981) it was
332 assumed that the limitation of RuBP regeneration could be adequately modelled by an
333 electron transport limitation without consideration of limitations by other PCR cycle enzymes.
334 This is probably the case in most instances however in transgenic studies care needs to be
335 taken. Transgenic tobacco with reduced sedoheptulose 1,7 bisposphatase (SBPase)
336 regeneration of RuBP has been shown to be the more limiting step (Harrison *et al.*, 2001;
337 Harrison *et al.*, 1998). In the case of C_4 photosynthesis the possibility that PEP regeneration
338 may also be limited by the enzyme activity of enzymes such as PPDK and malic enzyme at high
339 irradiance has also been found in transgenic studies with *Flaveria bidentis* a C_4 dicot (Furbank
340 *et al.*, 2001; Pengelly *et al.*, 2012; Trevanion *et al.*, 1997). C_4 transgenic plants with altered
341 RuPB regeneration capacity have not yet been reported on.

bioRxiv preprint doi: https://doi.org/10.1101/2021.03.13.435281; this version posted March 14, 2021. The copyright holder for this preprint (which was not certified by peer review) is the author/funder. All rights reserved. No reuse allowed without permission.

An update on the parameterisation of the C_4 photosynthesis model

This model is built on the same principal as the Farquhar et al. (1980) model and many of the model's parameters can be assigned a priori and this is indicated in Table 1, leaving only key variables like V_{cmax} V_{pmax}, V_{pr}, and J_{max} to be assigned. It is however important to note that the kinetic constants of Rubisco from C_4 species differ from those of C_3 species and vary amongst the different C_4 decarboxylation types (Badger *et al.*, 1974; Ghannoum *et al.*, 2005; Jordan and Ogren, 1981, 1983; Sharwood *et al.*, 2016).

The C_4 monocot species *Setaria viridis* (green foxtail millet), a NADP-malic enzyme type which is closely related to agronomically important C_4 crops including *Setaria italica* (foxtail millet), *Z. mays* (maize), *Sorghum bicolor* (sorghum) and *Saccharum officinarum* (sugarcane) has been suggested as a new model species (Brutnell *et al.*, 2010). It has become a popular model species due to its rapid generation time, small stature, high seed production, diploid status and small sequenced and publicly available genome and it can be readily transformed (Alonso-Cantabrana *et al.*, 2018; Brutnell *et al.*, 2010; Doust, 2007; Li and Brutnell, 2011; Osborn *et al.*, 2016). This has led to excellent biochemical characterisation of *S. viridis* PEPC and Rubisco (Boyd *et al.*, 2015; DiMario and Cousins, 2019). Most parameters were taken from Boyd et al. (2015), but the Michaelis Menten constant for CO_2 , K_p, was updated with more recent measurements by Di Mario and Cousins (2019). It is important to note that PEPc fixes bicarbonate rather than CO_2 and K_p is converted from measured values of K_m for HCO_3^- [1]. Here a cytosolic pH of 7.2 and pKa =6.12 was assumed (Hatch and Burnell, 1990). The precise value of cytosolic pH is unknown and if a pH of 7.4 is assumed K_p decreases from 82 µbar to 50 µbar. PEPc S. viridis RNAi line has been used to characterise bundle-sheath conductance to CO_2 diffusion (g_{bs}) and its temperature dependence (Alonso-Cantabrana *et al.*, 2018). This has for the first time provided a cohesive parameter set and the associated temperature functions (Table 1).

It is best to estimate the temperature response of J_{max} from a series of light response curves made at high CO_2 and different temperatures as was done by Massad et al (2007) for *Zea mays*. They used an Arrhenius function for their parameterisation. The simpler temperature function suggested by June et al. (2004) is used here to parametrise the temperature dependence of electron transport (Table 1) and the parameterisation for tobacco has been used (Yamori *et al.*, 2010) since these experiments still need to be done for *S. viridis.*

bioRxiv preprint doi: https://doi.org/10.1101/2021.03.13.435281; this version posted March 14, 2021. The copyright holder for this preprint (which was not certified by peer review) is the author/funder. All rights reserved. No reuse allowed without permission.

Sonawane et al. (2017), who characterised the temperature response of CO_2 assimilation rate in a number of C_4 grasses used this function to fit the saturated rate of CO_2 assimilation measured at high irradiance. The tobacco values chosen here fit within the range values reported for these C_4 grasses (Sonawane *et al.*, 2017)

Calculating the electron transport required to sustain CO_2 assimilation

Von Caemmerer and Farquhar (1981) suggested that measurements of CO_2 assimilation rate can be used to calculate the electron transport rate needed to support the CO_2 assimilation rate. Equation 37 can be used in the same way. Using equation 39 to solve for J_t this results in the following quadratic equation:

$$J = \left(-b + \sqrt{b^2 - 4ac}\right)/(2a) \quad (46)$$

$$a = z^2 \frac{x}{2} \frac{1-x}{3} \quad (47)$$

$$b = \frac{z(1-x)}{3}[g_{sb}(C_m - \gamma_* O_m) - R_m - A(1 - \gamma_* \alpha)] - \frac{zx}{2}(A + R_d) \quad (48)$$

$$c = (A + R_d)[R_m - g_{sb}(C_m + \gamma_* O_m\, 7/3) + A(1 - \gamma_* \alpha\, 7/3)] \quad (49)$$

These equations were introduced by Ubierna et al.(2013) for linear electron flow only (z=0.75) and the assumption of 3 H^+=/ATP.

Model evaluation

Modelled CO_2 response of CO_2 assimilation

In C_3 species CO_2 response curves are widely used to assess photosynthetic capacity (Ainsworth and Rogers, 2007; Sharkey *et al.*, 2007; von Caemmerer, 2000; von Caemmerer and Farquhar, 1981). Figure 3 compares the model output of the Farquhar, von Caemmerer and Berry model of C_3 photosynthesis (Farquhar *et al.*, 1980) with the current C_4 model presented here. In the C_3 model the enzyme limited rate is dominated by Rubisco and its kinetic parameters at low CO_2 and the electron transport capacity limits at high CO_2 (Fig. 3a). In the C_4 model it is also possible to distinguish an enzyme limited CO_2 assimilation rate at high light (equations 20-25) and an electron transport limited rate (equations 37-44). However, the enzyme limited rate is determined by PEPC at low CO_2 and Rubisco at high

bioRxiv preprint doi: https://doi.org/10.1101/2021.03.13.435281; this version posted March 14, 2021. The copyright holder for this preprint (which was not certified by peer review) is the author/funder. All rights reserved. No reuse allowed without permission.

399 CO_2. The electron transport limited rate can also determine the CO_2 assimilation rate at high
400 CO_2 (Fig. 3b). Thus, it is more difficult to identify biochemical limitations to C_4
401 photosynthesis.

402 Usually good correlations are found between in vitro Rubisco activity and the CO_2 saturated
403 rate of CO_2 assimilation rate at high CO_2 (Sonawane *et al.*, 2017; Usuda, 1984; Usuda *et al.*,
404 1984). The relationship should be almost one to one as Rubisco operates close to its
405 saturated rate in vivo. In the study of *Flaveria bidentis* transgenics with varying reductions in
406 Rubisco content show a slight curylinear relationship between Rubisco content and CO_2
407 assimilation rate hinting at a possible electron transport limitation in wild type plants
408 (Furbank *et al.*, 1996; von Caemmerer *et al.*, 1997). These studies have also provided
409 evidence that Rubisco limits CO_2 assimilation at high CO_2. Transgenic plants with reduced
410 Rubisco content showing a clear decline in CO_2 assimilation rate at high CO_2 (Pengelly *et al.*,
411 2012; von Caemmerer *et al.*, 1997). Recent photosynthetic engineering that increased
412 Rubisco content in maize leaves resulted in an increase in CO_2 saturated CO_2 assimilation
413 rate (Salesse-Smith *et al.*, 2018).

414 Here the model has been tuned in such a way that at 25 °C electron transport rate is limiting
415 CO_2 assimilation at high CO_2 and high irradiance. This balance can of course vary with
416 growth conditions or species, but there is no straight forward technique to determine the
417 limitation. Furthermore, the assumption has been made the electron transport capacity and
418 PEP and RuBP regeneration generally co-limit. In transgenic studies where regeneration of
419 the C_4 cycle has been curtailed by molecular manipulation, it is clear that this also limits CO_2
420 assimilation at high CO_2 (Pengelly *et al.*, 2012; Trevanion *et al.*, 1997). In a study, transgenic
421 *S. viridis* with overexpression of the Rieske iron sulphur protein in the cytochrome b_6f
422 complex had increased CO_2 assimilation rates at ambient and high CO_2 confirming that
423 electron transport capacity can limit CO_2 assimilation rate (Ermakova *et al.*, 2019). The fact
424 that electron transport rate limits CO_2 assimilation rate at high CO_2 means that a reduction
425 in irradiance is also predicted to primarily affects the CO_2 saturated rate of CO_2 assimilation
426 rather than the initial slope of the CO_2 response curve except at low irradiance (Leegood
427 and von Caemmerer, 1989; Pfeffer and Peisker, 1998).

bioRxiv preprint doi: https://doi.org/10.1101/2021.03.13.435281; this version posted March 14, 2021. The copyright holder for this preprint (which was not certified by peer review) is the author/funder. All rights reserved. No reuse allowed without permission.

There are three possible limitations to the initial slope of the CO_2 response curve; the mesophyll conductance to CO_2 diffusion from intercellular airspace to the mesophyll cytosol g_m; the rate of CO_2 hydration by carbonic anhydrase, CA, and the rate of PEP carboxylation. It is thought that most C_4 leaves have sufficient CA for it not to be rate limiting (Cousins *et al.*, 2008; Hatch and Burnell, 1990). However, studies with transgenic or mutant plants in *Flaveria bidentis*, *Zea mays* and *Setaria viridis* have shown that when CA activity is greatly reduced a reduction in initial slope of the CO_2 response is observed (Osborn *et al.*, 2016; Studer *et al.*, 2014; von Caemmerer *et al.*, 2004).

The initial C_4 photosynthesis models did not consider a diffusion limitation between the intercellular airspace and the mesophyll cytosol. In C_4 species mesophyll conductance , g_m, is likely to be proportional to mesophyll surface area exposed to intercellular airspace (Evans and von Caemmerer, 1996). The standard techniques used to quantify mesophyll conductance in C_3 species such as combined measurements of gas exchange and chlorophyll fluorescence, or measurements of ^{13}C isotope discrimination cannot be used in C_4 species, however a new technique has been developed to measure mesophyll conductance in C_4 species using $C^{18}O^{16}O$ isotope discrimination (Barbour *et al.*, 2016; Gillon and Yakir, 2000; Ogée *et al.*, 2018; Osborn *et al.*, 2016) and here the temperature dependence of g_m measured for *Setaria viridis* has been used for parameterisation of the model (Table 1, Ubierna *et al.*, 2017).

The drop in CO_2 partial pressure from intercellular airspace, C_i to that of the mesophyll, C_m are related in the following equation

$$A = g_m(C_i - C_m). \quad (50)$$

Incorporating equation (50) into equation (21) results in a cubic expression which is not easily solved. It can be incorporated into equation (40) giving a slightly more complex quadratic. In case of the initial slope of the CO_2 response curve one can use equation (26) and ignoring the term g_sC_m and combining it with equation (50) a quadratic similar to the one given for C_3 leaves is obtained (von Caemmerer, 2000; von Caemmerer and Evans, 1991).

$$A^2 - A\left(g_m\left(C_i + K_p\right) + V_{pmax} - R_m\right) + g_m\left(V_{pmax}C_i - R_m\left(C_i + K_p\right)\right) = \quad (51)$$

bioRxiv preprint doi: https://doi.org/10.1101/2021.03.13.435281; this version posted March 14, 2021. The copyright holder for this preprint (which was not certified by peer review) is the author/funder. All rights reserved. No reuse allowed without permission.

456 The first derivative with respect to C_i at C_i=0 is given by

457 $$\frac{dA}{dc_i} = \frac{g_m V_{pmax}}{g_{mK_p+} V_{pmax}} \quad (52)$$

458 Pfeffer and Peisker (1988 and 1998) used this equation together with measurements of PEP
459 carboxylase activity and initial slope (dA/dC_i) to estimate g_m in plants grown under different
460 light intensities. Figure 4 shows the effect inclusion of mesophyll conductance has on the
461 initial slope. Equation 52 was used by Ubierna et al. (2016) to estimate g_m from in vitro
462 measurements of PEP carboxylase activity, $V_{pmax,}$ and they found good agreement with
463 estimates of g_m from measurements of $C^{18}O^{16}O$ isotope discrimination, however the
464 uncertainties surrounding estimates of K_p discussed above need to be considered.

465 Strong correlations between leaf nitrogen, CO_2 assimilation rate and PEP carboxylase activity
466 have been observed in several studies (Meinzer and Zhu, 1998; Sage and Pearcy, 1987; Usuda,
467 1984; Wong *et al.*, 1985) however it has been more difficult to provide quantitative
468 correlations. Without the inclusion of a mesophyll conductance estimates of V_{pmax} form the
469 initial slope are often less than what is measured in vitro. For example if the initial slope of
470 the lower curve in Figure 4a is used to estimate V_{pmax} with an infinitely large g_m the predicted
471 V_{pmax} is 58 µmol m^{-2} s^{-1} whereas it has here been modelled with a V_{pmax} of 200 µmol m^{-2} s^{-1}
472 and gm = 1 mol m^{-2} s^{-1} bar^{-1}. Hence mesophyll conductance is an important parameter in
473 linking C_4 biochemistry with gas exchange.

474 ## Modelled light response of CO_2 assimilation

475 It is well recognised that the light response of C_4 photosynthesis does frequently not
476 saturate (Cousins *et al.*, 2006; Leakey *et al.*, 2006). Figure 5 shows typical modelled light
477 response curves of CO_2 assimilation rate at several mesophyll CO_2 partial pressures. In the
478 current parametrisation CO_2 assimilation rate is electron transport limited at all irradiances
479 above C_m=150 µbar at 25 °C. The shapes of the curves are determined by equation (34)
480 which as for the C_3 photosynthetic model remains empirical and the partition partitioning of
481 electron transport between C_4 and C_3 cycle has been set at x=0.4 (equation 29). Furbank
482 and von Caemmerer gave a detailed discussion about the optimal partitioning of electron
483 transport capacity between C_3 and C_4 cycle (Peisker, 1988; von Caemmerer, 2000; von
484 Caemmerer and Furbank, 1999). It is noteworthy that the fraction of electron transport

bioRxiv preprint doi: https://doi.org/10.1101/2021.03.13.435281; this version posted March 14, 2021. The copyright holder for this preprint (which was not certified by peer review) is the author/funder. All rights reserved. No reuse allowed without permission.

allocated to the C_4 cycle, x, equals 0.4 over a wide range of irradiances but drops at very low irradiance. Under low light the bundle-sheath CO_2 partial pressures are close to the mesophyll CO_2 partial pressure and electron transport is required for recycling of photo respiratory CO_2. The optimal partitioning increases from 0.404 to 0.417 if oxygen is evolved in the bundle sheath (α=1). It also declines slightly with increasing temperature as Rubisco specificity for CO_2 decreases (Jordan and Ogren, 1984; Sharwood *et al.*, 2016).

In C_3 species there a close link has been established between chloroplast electron transport capacity and electron transport chain intermediates such as cytochrome f (Yamori *et al.*, 2010). In C_4 photosynthesis this quantitative link between cytochrome f content and electron transport capacity needs also to be investigated.

Modelled temperature response of CO_2 assimilation rate

C_4 plants have higher CO_2 assimilation rates at high temperatures and higher photosynthetic temperature optima than their C_3 counterparts largely because of the elimination of photorespiratory CO_2 losses. (Berry and Björkman, 1980; Long, 1999). The temperature response of electron transport is not well characterised in C_4 species. With the parameterisation used here, CO_2 assimilation rate is electron transport limited above 25°C, and enzyme limited below a Ci=150 µbar at hight light, which corresponds to the operating C_i of many C_4 species at ambient CO_2 (Figure 6). There is some evidence that this is not unreasonable. Figure 7 shows a comparison of a temperature response of CO_2 assimilation rate of *Flaveria bidentis* wildtype and transgenic Flaveria with reduced Rubisco content (Kubien *et al.*, 2003). In Figure 7b CO_2 assimilation rate is expressed on a Rubisco site basis (in vivo k_{cat}) and compared the temperature response of Rubisco in vitro activity. For Flaveria with reduced amount of Rubisco there is a match between in vivo and in vitro k_{cat} up to approximately 30°C whereas for the wild type in vivo k_{cat} is less than the in vitro Rubisco k_{cat} around 20°C indicating other limitations to CO_2 assimilation rate such as electron transport capacity. Temperature optima of CO_2 assimilation rate are dependent on growth environment (Berry and Björkman, 1980; Dwyer *et al.*, 2007). The modelling suggests that the temperature optimum is most likely determined by the properties of the electron transport capacity (Figure 6).

bioRxiv preprint doi: https://doi.org/10.1101/2021.03.13.435281; this version posted March 14, 2021. The copyright holder for this preprint (which was not certified by peer review) is the author/funder. All rights reserved. No reuse allowed without permission.

In Figure 8a the CO_2 response curves have been modelled for different leaf temperatures. Figure 8a, shows that at low temperature the CO_2 response is enzyme limited at all Ci, as temperature is increased the transition from enzyme limited CO_2 assimilation rate to electron transport limited rate occurs at progressively lower C_i. There is an increase in initial slope with increasing temperature which is caused by the temperature response of the mesophyll conductance and the different temperature dependencies of maximal PEPC carboxylation and is Michaelis Menten constant (V_{pmax} and K_p) (Figure 8 a and b, Table 1). These model predictions fit well with experimental observations by Sonawane et al.(2017).

A note on leakiness

The bundle sheath resistance or its inverse the bundle sheath conductance to CO_2 diffusion are key parameters that together with relative capacities for the C_4 cycle and Rubisco and electron transport capacity determine the effectiveness of the CO_2 concentration mechanism. This is often quantified by a term called leakiness (ϕ), which is defined as the ratio of the rates of CO_2 leakage out of the bundle sheath over the rate of CO_2 supply to the bundle sheath (equation 4 and 5). Carbon isotope discrimination can be used to determine leakiness (Farquhar, 1983). Combined measurements of gas exchange and carbon isotope discrimination have been used to assess leakiness under different environmental conditions (Henderson *et al.*, 1992; King *et al.*, 2012; Kromdijk *et al.*, 2010; Pengelly *et al.*, 2010; Sun *et al.*, 2012; Ubierna *et al.*, 2011; von Caemmerer and Furbank, 2003). It is tempting to predict leakiness from the C_4 photosynthesis model, but because it is a flux model little can be said about the rate of the component that is not limiting and leakiness estimates are not realistic as non-rate limiting steps are likely to be down regulated. However, when CO_2 assimilation rates and leakiness are known from combined measurements of gas exchange and carbon isotope discrimination the model can be used to calculated the rate of the C_4 cycle and the leak rate from the following equations and equation 4

$$V_p = \frac{A+R_m}{1-\phi}. \qquad (53)$$

With the assumption of a bundle sheath conductance bundle sheath CO_2 can also be estimated (Pengelly *et al.*, 2012).

bioRxiv preprint doi: https://doi.org/10.1101/2021.03.13.435281; this version posted March 14, 2021. The copyright holder for this preprint (which was not certified by peer review) is the author/funder. All rights reserved. No reuse allowed without permission.

Conclusion

The steady state C_4 photosynthesis model has been updated and parameterized with the *in vitro* kinetic constants for Rubisco and PEP carboxylase and values for mesophyll and bundle sheath conductance and their temperature dependencies. Furthermore, electron transport rate equations have been updated to include cyclic electron transport flow. Now it is important to compare gas exchange measurements and biochemical measurements to confirm the quantitative relationships predicted by the model. In particular a parameterization of the temperature response of electron transport rate is needed and information of how it relates to thylakoid electron transport components such as the b_6f complex which has shown to be a good correlator of C_3 photosynthetic electron transport.

Acknowledgment

I thank Robert T Furbank and Alex Wu for helpful comments on this manuscript. This research was supported by the Australian Research Council (ARC) Centre of Excellence for Translational Photosynthesis (CE140100015).

Table 1. Photosynthetic parameters used in the model. When available values for *Setaria viridis* have been chosen.

Parameter	Value at 25°C	Definition	Activation energy E (kJmol^{-1})	Reference
V_{cmax}	40 μmol m^{-2} s^{-1} or variable	maximum Rubisco activity	78[c]	(Boyd *et al.*, 2015)
K_c	1210 μbar	Michaelis constant of Rubisco for CO_2	64.2	(Boyd *et al.*, 2015)
K_o	292 mbar	Michaelis constant of Rubisco for O_2	10.5	(Boyd *et al.*, 2015)
$\gamma*$	=0.0003817 (0.5/2619)	0.5/($S_{c/o}$) half the reciprocal of Rubisco specificity	31.1	(Boyd *et al.*, 2015)
V_{pmax}	300 μmol m^{-2} s^{-1} or variable	maximum PEP carboxylase activity	94.8	(Boyd *et al.*, 2015)
V_{pr}	80 μmol m^{-2} s^{-1} or variable	PEP regeneration rate		
K_p	82 μbar	Michaelis constant of PEP carboxylase for CO_2	36.3	(DiMario and Cousins, 2019)
g_{bs}	0.003 mol m^{-2} s^{-1} bar-1	bundle sheath conductance to CO_2	Constant with temperature	(Alonso-Cantabrana *et al.*, 2018)
g_o	0.047 g_s	bundle sheath conductance to O_2		(Farquhar, 1983)
R_d	0.01*V_{cmax}	Leaf mitochondrial respiration	66.4	(Farquhar *et al.*, 1980)
R_m	0.5 R_d	mesophyll mitochondrial respiration		
α	0<α>1,	fraction of PSII activity in the bundle sheath		
x	0.4	partitioning factor of electron transport rat		
J_{max}	170 μmol electrons m^{-2}s^{-1} or variable	maximal linear electron transport rate		
T_o	43°C	T optimum	$J_{max}(T_L) = J_{max}(T_o)e^{-\left(\frac{T_L - T_o}{\Omega}\right)^2}$	(June *et al.*, 2004; Yamori *et al.*, 2010)
Ω	26	Ω is the difference in temperature from T_o at which J falls to e^{-1} (0.37)		(Yamori *et al.*, 2010)
J_{max}@ T_o	300 μmol electrons m^{-2}s^{-1} or variable			
h	4	Number of protons per ATP		
f_{cyc}	0.5 or variable	Fraction of cyclic electron transport		(Yin and Struik, 2012)
z		Ratio of the rate of ATP production to linea electron transport (J_{ATP}/J)		(Yin and Struik, 2012)
g_m	1 mol m^{-2} s^{-1} bar^{-1}	Mesophyll conductance to CO_2	40.6	(Ubierna *et al.*, 2017)

[C] Values of parameters where activation energies have been given can be calculated at any temperature from the following equation: $Parameter\ (25℃)exp[(T-298)E/298RT]$, where R (8.314JK^{-1}mol^{-1}) is the universal gas constant and T is temperature in degrees Kelvin (K).

bioRxiv preprint doi: https://doi.org/10.1101/2021.03.13.435281; this version posted March 14, 2021. The copyright holder for this preprint (which was not certified by peer review) is the author/funder. All rights reserved. No reuse allowed without permission.

Figure legends

Figure 1

Schematic representing the main features of the C_4 photosynthetic pathway. CO_2 diffuses into the mesophyll where it is converted to HCO_3^- and fixed by PEP carboxylase at the rate V_p. In the steady state C_4 acid decarboxylation occurs at the same rate. CO_2 released in the bundle sheath either leaks out of the bundle sheath at (L) or is fixed by Rubisco (V_c). In the photosynthetic carbon oxidation cycle CO_2 is released at the half the oxygenation rate (V_o). CO_2 is also released by respiration (R_m, R_s) in mesophyll and bundle sheath respectively. Electron transport components are not shown.

Figure 2

Scheme for linear and cyclic electron transport in the light reactions of photosynthesis. The arrows indictate electron transport. Thick curved arrows show the number of protons produced per electron transported. J denotes linear electron transport through photosystem II, J_1 is electron transport trough photosystem I and J_{cyc} the rate of cyclic electron transport. The symbol f_{cyc} denotes the fraction of J_1 that flows via the cyclic mode. The diagram has been adapted from Yin et al. (2004).

Figure 3

A comparison of modelled rates of CO_2 assimilation rate as functions of partial pressures of CO_2 for C_3 (a) and C_4 photosynthesis (b).

a) Modelled rate of CO_2 assimilation as a function of chloroplast CO_2 partial pressure for the C_3 photosynthetic pathway at 25 °C. The Rubisco limited (RuBP saturated rate) of CO_2 assimilation has a dashed line extension at high CO_2. The electron transport (RuBP regeneration) limited rate of CO_2 assimilation has a dotted line extension at low CO_2. The solid curve represents the minimum rate that is the actual rate of CO_2 assimilation. A possible triose phosphate limitation at high CO_2 is not shown. (Redrawn from von Caemmerer 2000).
b) Modelled rate of CO_2 assimilation as a function of mesophyll cytosolic CO_2 partial pressure for the C_4 photosynthetic pathway at 25 °C and an irradiance of 1500 µmol m^{-2} s^{-1}. The enzyme limited CO_2 assimilation rate (PEPC limitation at low CO_2 and Rubisco limitation at high CO_2 shows the Rubisco limited rate as a dashes line extension. The electron transport (RuBP and PEP regeneration) limited rate of CO_2 assimilation has a dotted line extension at low CO_2. The solid curve represents the minimum rate that is the actual rate of CO_2 assimilation. Parameters used are given in Table 1.

Figure 4

The effect of mesophyll conductance, g_m on the initial slope of the CO_2 response curve.

a) Modelled rate of CO_2 assimilation as a function of intercellular CO_2 partial pressure for the C_4 photosynthetic pathway at 25 °C and an irradiance of 2000 µmol m^{-2} s^{-1}modelled with g_m =1 mol m^{-2} $s^{-1}$$bar^{-1}$ or an infinite g_m.
b) Initial slope (equation x) as a function of mesophyll conductance. Model parameters are those given in Table 1.

bioRxiv preprint doi: https://doi.org/10.1101/2021.03.13.435281; this version posted March 14, 2021. The copyright holder for this preprint (which was not certified by peer review) is the author/funder. All rights reserved. No reuse allowed without permission.

Figure 5

The effect of irradiance on modelled rate of CO_2 assimilation.

a) Light response of CO_2 assimilation rate at mesophyll cytosolic CO_2 partial pressures, C_m, in dictated in the figure. The C_4 photosynthesis model predicts electron transport limitations at all irradiance at C_m values above 150 µbar. At lower C_m, CO_2 assimilation rates are enzyme limited at high irradiance. The model was parameterised at 25 °C with values given in Table 1 and x=0.4.

b) CO_2 assimilation rate as a function of intercellular CO_2 at irradiances indicated. The model was parameterised at 25 °C with values given in Table 1 and x=0.4.

Figure 6

Modelled CO_2 assimilation rate as a function of leaf temperature. The dotted line and its extension line show the enzyme limited rate and the dashed line and its extension line show the electron transport limited rate. CO_2 assimilation rate was modelled at an irradiance of 2000 µmol m^{-2} s^{-1} and mesophyll CO_2, C_m of 150 µbar. Other parameters are as given in Table 1.

Figure 7

a) Temperature responses CO_2 assimilation rate in *Faveria bidentis* wild type and anti-Rubisco plants Photosynthesis was measured at different leaf temperatures and ambient CO_2 of 370 µbar and 200 mbar O_2 and an irradiance of 1500 µmol m^{-2} s^{-1}. Each point represents the mean (± SE) of measurements on five different leaves.

b) Temperature dependence of the in vitro and in vivo k_{cat} for Rubisco in wildtype and anti-Rubisco *F. bidentis*. The in vitro data reflect the activity of the fully carbamylated enzyme; in vivo k_{cat} is estimated as gross photosynthesis divided by the number of Rubisco catalytic sites. Each value represents the mean (± SE) of four measurements.

The data is redrawn from Figures 1 and 4 (Kubien *et al.*, 2003)

Figure 8

a) Modelled rate of CO_2 assimilation as a function of intercellular CO_2 partial pressure, C_i, for the C_4 photosynthetic pathway at three leaf temperatures of 15, 25 and 35°C and an irradiance of 2000 µmol m^{-2} s^{-1}. At 15°C CO_2 assimilation rate is enzyme limited at all C_i. For 25 and 35°C the arrow indicates the transition from enzyme limitation at low C_i to electron transport limitation at high C_i. Parameters used are given in Table 1.

b) Intial slope (dA/dC_i) calculated from equation 52 as a function of leaf temperature. Parameters used are given in Table 1.

bioRxiv preprint doi: https://doi.org/10.1101/2021.03.13.435281; this version posted March 14, 2021. The copyright holder for this preprint (which was not certified by peer review) is the author/funder. All rights reserved. No reuse allowed without permission.

Figures

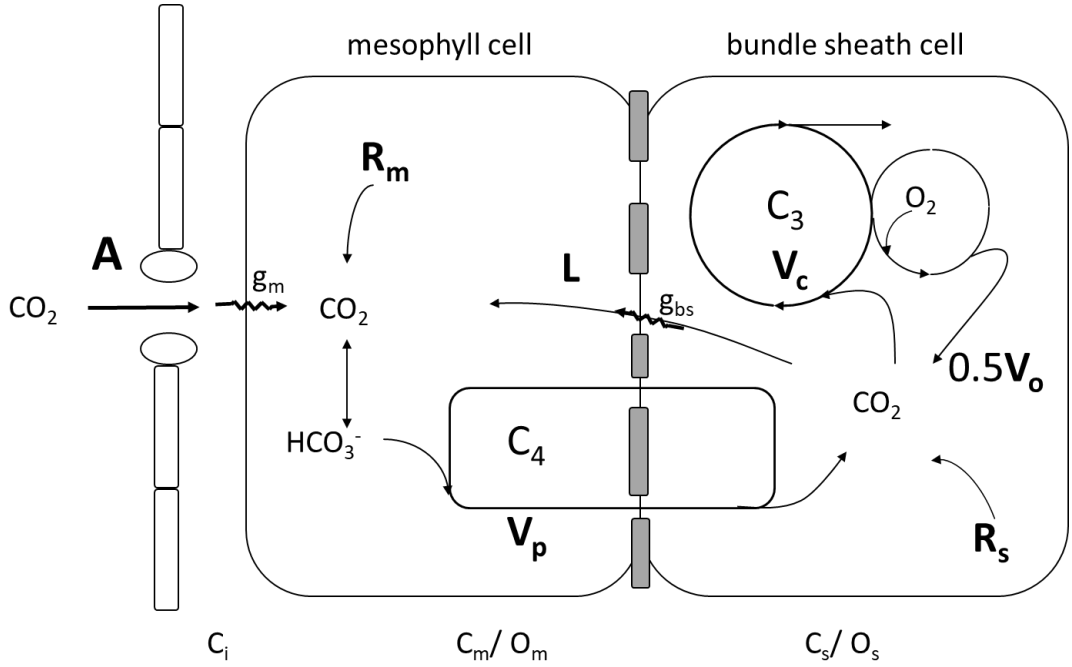


Figure 1

Schematic representing the main features of the C_4 photosynthetic pathway. CO_2 diffuses into the mesophyll where it is converted to HCO_3^- and fixed by PEP carboxylase at the rate V_p. In the steady state C_4 acid decarboxylation occurs at the same rate. CO_2 released in the bundle sheath either leaks out of the bundle sheath at (L) or is fixed by Rubisco (V_c). In the photosynthetic carbon oxidation cycle CO_2 is released at the half the oxygenation rate (V_o). CO_2 is also released by respiration (R_m, R_s) in mesophyll and bundle sheath respectively. Electron transport components are not shown.

bioRxiv preprint doi: https://doi.org/10.1101/2021.03.13.435281; this version posted March 14, 2021. The copyright holder for this preprint (which was not certified by peer review) is the author/funder. All rights reserved. No reuse allowed without permission.

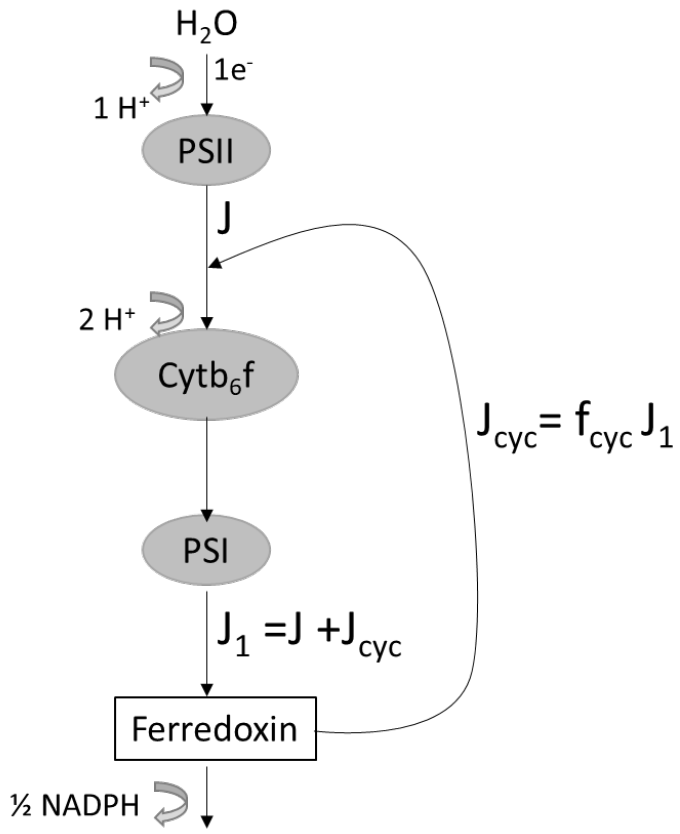


Figure 2

Scheme for linear and cyclic electron transport in the light reactions of photosynthesis. The arrows indictate electron transport. Thick curved arrows show the number of protons produced per electron transported. J denotes linear electron transport through photosystem II, J_1 is electron transport trough photosystem I and J_{cyc} the rate of cyclic electron transport. The symbol f_{cyc} denotes the fraction of J_1 that flows via the cyclic mode. The diagram has been adapted from Yin et al. (2004).

bioRxiv preprint doi: https://doi.org/10.1101/2021.03.13.435281; this version posted March 14, 2021. The copyright holder for this preprint (which was not certified by peer review) is the author/funder. All rights reserved. No reuse allowed without permission.

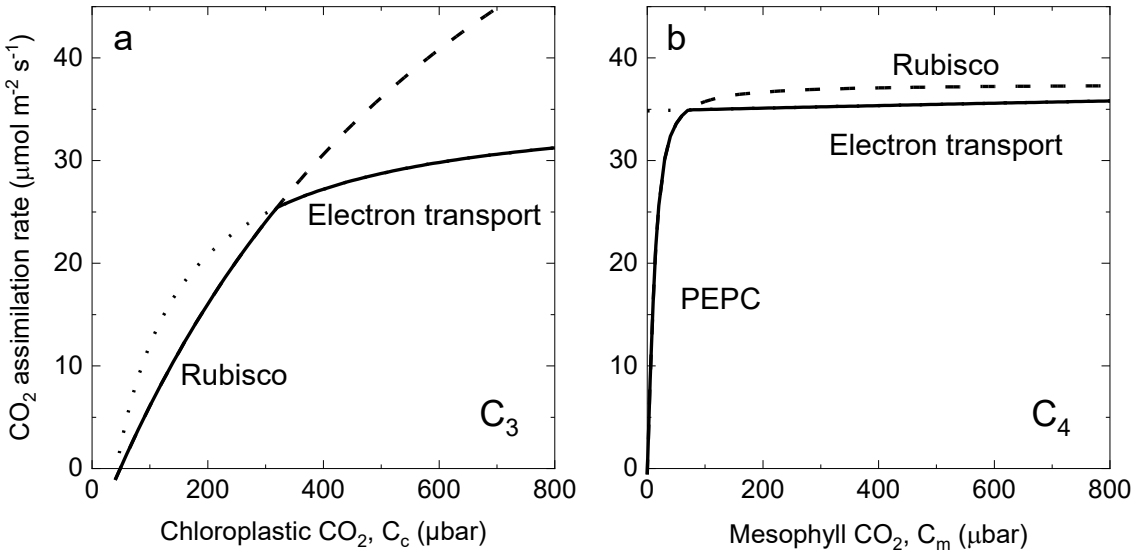


Figure 3

A comparison of modelled rates of CO_2 assimilation rate as functions of partial pressures of CO_2 for C_3 (a) and C_4 photosynthesis (b).

c) Modelled rate of CO_2 assimilation as a function of chloroplast CO_2 partial pressure for the C_3 photosynthetic pathway at 25 °C. The Rubisco limited (RuBP saturated rate) of CO_2 assimilation has a dashed line extension at high CO_2. The electron transport (RuBP regeneration) limited rate of CO_2 assimilation has a dotted line extension at low CO_2. The solid curve represents the minimum rate that is the actual rate of CO_2 assimilation. A possible triose phosphate limitation at high CO_2 is not shown. (Redrawn from von Caemmerer 2000).

d) Modelled rate of CO_2 assimilation as a function of mesophyll cytosolic CO_2 partial pressure for the C_4 photosynthetic pathway at 25 °C and an irradiance of 1500 µmol m^{-2} s^{-1}. The enzyme limited CO_2 assimilation rate (PEPC limitation at low CO_2 and Rubisco limitation at high CO_2 shows the Rubisco limited rate as a dashes line extension. The electron transport (RuBP and PEP regeneration) limited rate of CO_2 assimilation has a dotted line extension at low CO_2. The solid curve represents the minimum rate that is the actual rate of CO_2 assimilation. Parameters used are given in Table 1.

bioRxiv preprint doi: https://doi.org/10.1101/2021.03.13.435281; this version posted March 14, 2021. The copyright holder for this preprint (which was not certified by peer review) is the author/funder. All rights reserved. No reuse allowed without permission.

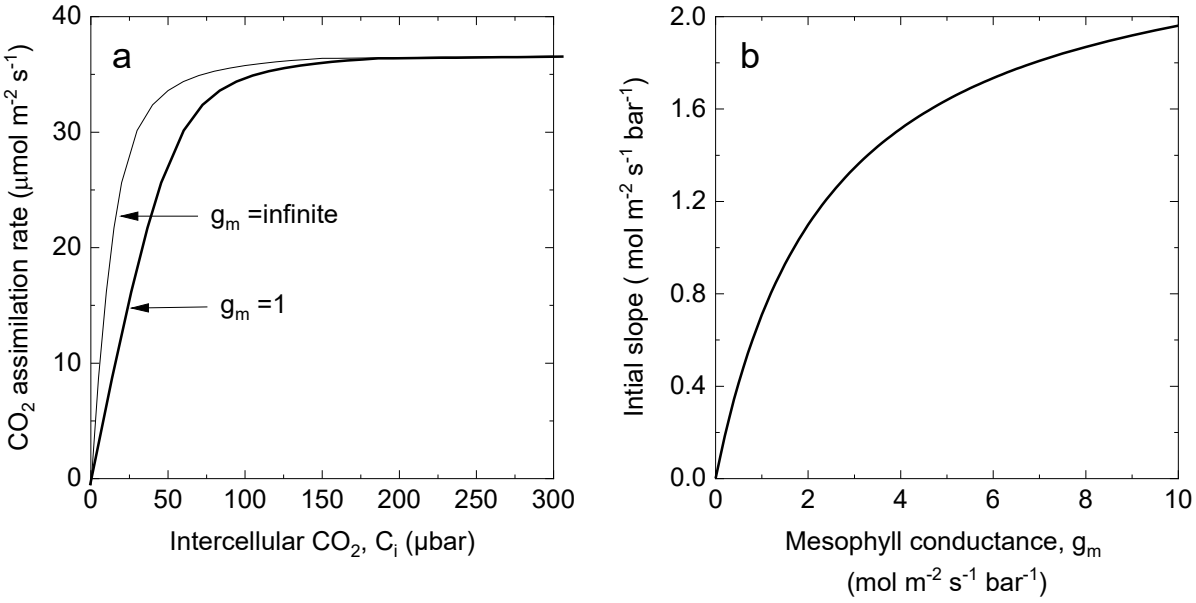


Figure 4

The effect of mesophyll conductance, g_m on the initial slope of the CO_2 response curve.

a) Modelled rate of CO_2 assimilation as a function of intercellular CO_2 partial pressure for the C_4 photosynthetic pathway at 25 °C and an irradiance of 2000 µmol m^{-2} s^{-1}modelled with g_m =1 mol m^{-2} $s^{-1}$$bar^{-1}$ or an infinite g_m.
b) Initial slope (equation x) as a function of mesophyll conductance. Model parameters are those given in Table 1.

bioRxiv preprint doi: https://doi.org/10.1101/2021.03.13.435281; this version posted March 14, 2021. The copyright holder for this preprint (which was not certified by peer review) is the author/funder. All rights reserved. No reuse allowed without permission.

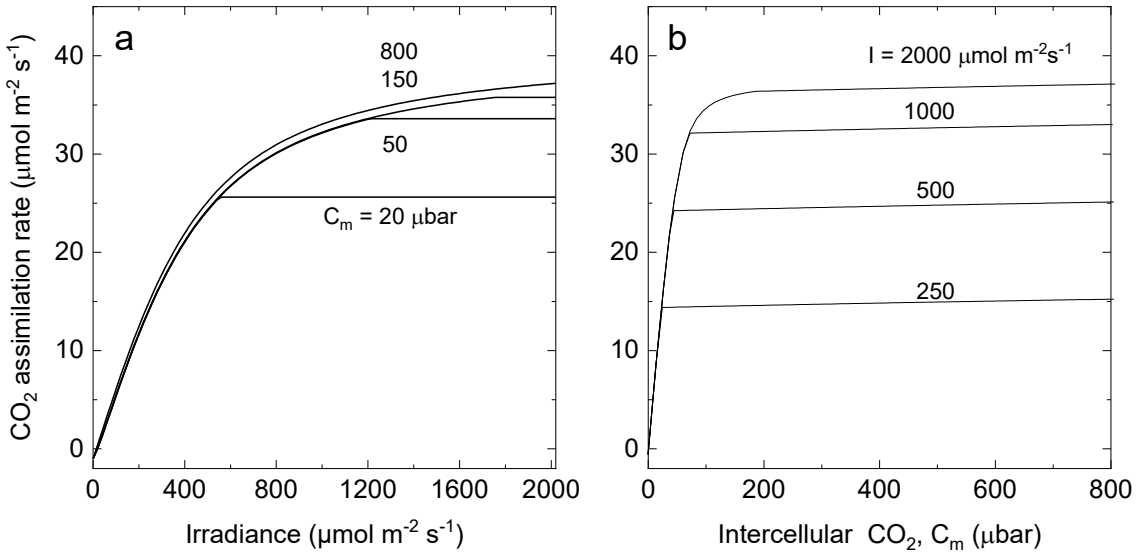


Figure 5

The effect of irradiance on modelled rate of CO_2 assimilation.

c) Light response of CO_2 assimilation rate at mesophyll cytosolic CO_2 partial pressures, C_m, in dictated in the figure. The C_4 photosynthesis model predicts electron transport limitations at all irradiance at C_m values above 150 μbar. At lower C_m, CO_2 assimilation rates are enzyme limited at high irradiance. The model was parameterised at 25 °C with values given in Table 1 and x=0.4.

d) CO_2 assimilation rate as a function of intercellular CO_2 at irradiances indicated. The model was parameterised at 25 °C with values given in Table 1 and x=0.4.

bioRxiv preprint doi: https://doi.org/10.1101/2021.03.13.435281; this version posted March 14, 2021. The copyright holder for this preprint (which was not certified by peer review) is the author/funder. All rights reserved. No reuse allowed without permission.

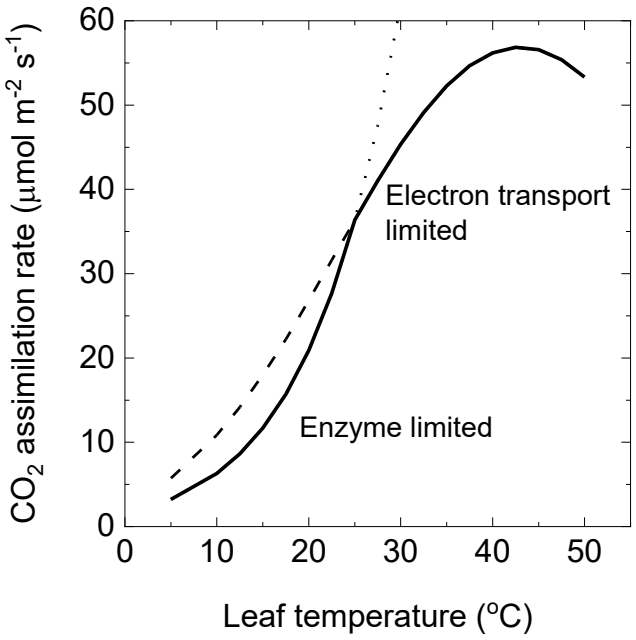


Figure 6

Modelled CO_2 assimilation rate as a function of leaf temperature. The dotted line and its extension line show the enzyme limited rate and the dashed line and its extension line show the electron transport limited rate. CO_2 assimilation rate was modelled at an irradiance of 2000 µmol m^{-2} s^{-1} and mesophyll CO_2, C_m of 150 µbar. Other parameters are as given in Table 1.

bioRxiv preprint doi: https://doi.org/10.1101/2021.03.13.435281; this version posted March 14, 2021. The copyright holder for this preprint (which was not certified by peer review) is the author/funder. All rights reserved. No reuse allowed without permission.

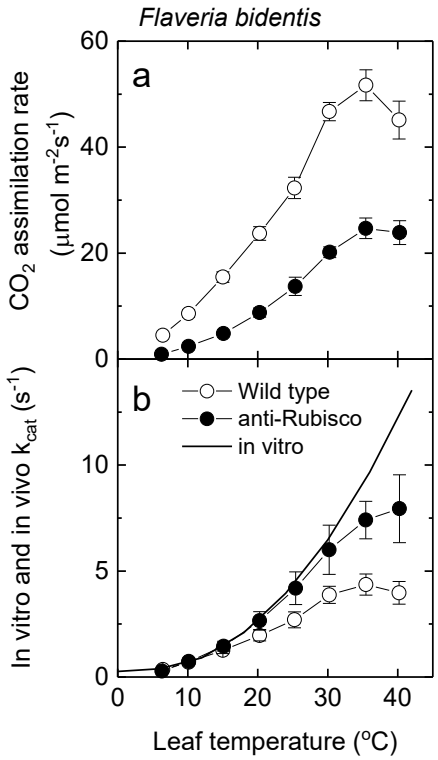


Figure 7

a) Temperature responses CO_2 assimilation rate in *Faveria bidentis* wild type and anti-Rubisco plants Photosynthesis was measured at different leaf temperatures and ambient CO_2 of 370 µbar and 200 mbar O_2 and an irradiance of 1500 µmol m^{-2} s^{-1}. Each point represents the mean (± SE) of measurements on five different leaves.

b) Temperature dependence of the in vitro and in vivo k_{cat} for Rubisco in wildtype and anti-Rubisco *F. bidentis*. The in vitro data reflect the activity of the fully carbamylated enzyme; in vivo k_{cat} is estimated as gross photosynthesis divided by the number of Rubisco catalytic sites. Each value represents the mean (± SE) of four measurements.

The data is redrawn from Figures 1 and 4 (Kubien *et al.*, 2003)

bioRxiv preprint doi: https://doi.org/10.1101/2021.03.13.435281; this version posted March 14, 2021. The copyright holder for this preprint (which was not certified by peer review) is the author/funder. All rights reserved. No reuse allowed without permission.

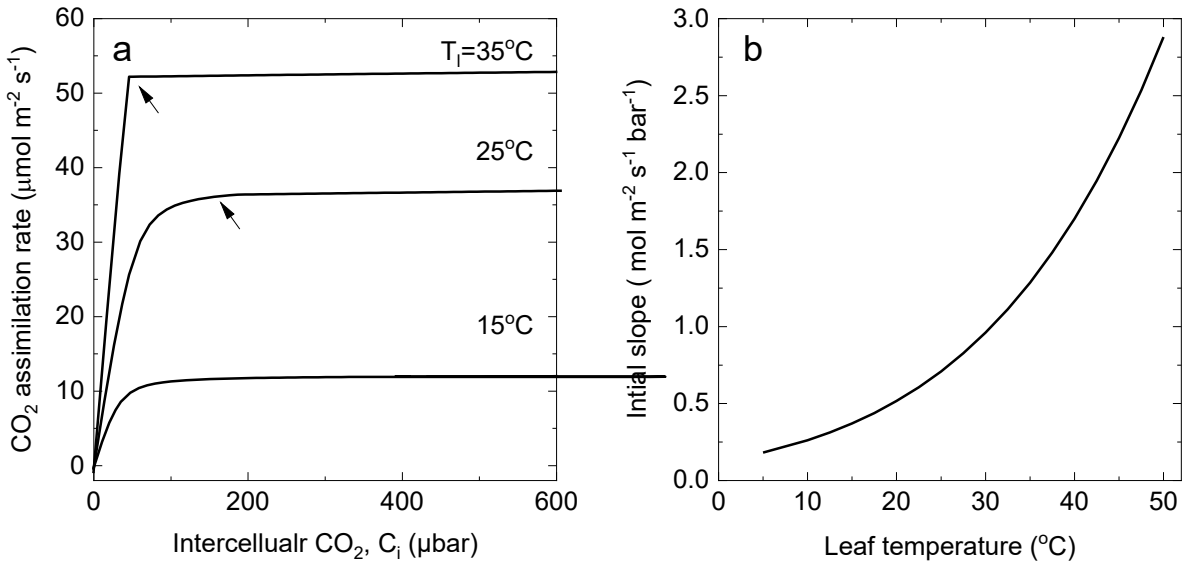


Figure 8

a) Modelled rate of CO_2 assimilation as a function of intercellular CO_2 partial pressure, C_i, for the C_4 photosynthetic pathway at three leaf temperatures of 15, 25 and 35°C and an irradiance of 2000 µmol m^{-2} s^{-1}. At 15°C CO_2 assimilation rate is enzyme limited at all C_i. For 25 and 35°C the arrow indicates the transition from enzyme limitation at low C_i to electron transport limitation at high C_i. Parameters used are given in Table 1.

b) Intial slope (dA/dC_i) calculated from equation 52 as a function of leaf temperature. Parameters used are given in Table 1.

bioRxiv preprint doi: https://doi.org/10.1101/2021.03.13.435281; this version posted March 14, 2021. The copyright holder for this preprint (which was not certified by peer review) is the author/funder. All rights reserved. No reuse allowed without permission.

References

Ainsworth EA, Rogers A. 2007. The response of photosynthesis and stomatal conductance to rising CO2 : mechanisms and environmental interactions. Plant Cell and Environment **30**, 258-270.

Alonso-Cantabrana H, Cousins AB, Danila F, Ryan T, Sharwood RE, von Caemmerer S, Furbank RT. 2018. Diffusion of CO_2 across the mesophyll-bundle sheath cell interface in a C_4 plant with genetically reduced PEP carboxylase activity. Plant Physiology **178**, 72-81.

Badger MR, Andrews TJ, Osmond CB. 1974. Detection in C_3, C_4 and CAM plant leaves of a low-$K_m(CO_2)$ form of RuDP carboxylase, having high RuDP oxygenase activity at physiological pH. In: Avron M, ed. *Proceedings of the Third International Congress on Photosynthesis*. Amsterdam: Elsevier, 1421-1429.

Barbour MM, Evans JR, Simonin KA, von Caemmerer S. 2016. Online CO_2 and H_2O oxygen isotope fractionation allows estimation of mesophyll conductance in C_4 plants, and reveals that mesophyll conductance decreases as leaves age in both C_4 and C_3 plants. New Phytologist **210**, 875-889

Bellasio C, Beerling DJ, Griffiths H. 2016. Deriving C4 photosynthetic parameters from combined gas exchange and chlorophyll fluorescence using an Excel tool: theory and practice. Plant, Cell & Environment **39**, 1164-1179.

Bellasio C, Quirk J, Buckley TN, Beerling D. 2017. A dynamic hydro-mechanical and biochemical model of stomatal conductance for C4 photosynthesis. Plant Physiology.

Berry JA, Björkman O. 1980. Photosynthetic response and adaptation to temperature in higher-plants. Annual Review of Plant Physiology and Plant Molecular Biology **31**, 491-543.

Berry JA, Farquhar GD. 1978. The CO_2 concentrating function of C_4 photosynthesis: a biochemical model. In: Hall D, Coombs J, Goodwin T, eds. *The Proceedings of the Fourth International Congress on Photosynthesis*. London: Biochemical Society of London, 119-131.

Boyd RA, Gandin A, Cousins AB. 2015. Temperature responses of C_4 photosynthesis: Biochemical analysis of Rubisco, Phosphoenolpyruvate Carboxylase, and Carbonic Anhydrase in *Setaria viridis*. Plant Physiology **169**, 1850-1861.

Brutnell TP, Wang L, Swartwood K, Goldschmidt A, Jackson D, Zhu XG, Kellogg E, Van Eck J. 2010. Setaria viridis: A Model for C_4 Photosynthesis. Plant Cell **22**, 2537-2544.

Chapman KSR, Berry JA, Hatch MD. 1980. Photosynthetic metabolism in bundle sheath cells of the C_4 species *Zea mays*: sources of ATP and NADPH and the contribution of photosystem 11. Archives of Biochemistry and Biophysics **202**, 330-341.

Collatz GJ, Ribas-Carbo M, Berry JA. 1992. Coupled photosynthesis-stomatal model for leaves of C_4 plants. Australian Journal of Plant Physiology **19**, 519-538.

Cousins AB, Badger MR, von Caemmerer S. 2006. Carbonic anhydrase and its influence on carbon isotope discrimination during C_4 photosynthesis. Insights from antisense RNA in Flaveria bidentis. Plant Physiology **141**, 232-242.

Cousins AB, Badger MR, von Caemmerer S. 2008. C_4 photosynthetic isotope exchange in NAD-ME- and NADP-ME-type grasses. Journal of Experimental Botany **59**, 1695-1703.

DiMario RJ, Cousins AB. 2019. A single serine to alanine substitution decreases bicarbonate affinity of phosphoenolpyruvate carboxylase in C_4Flaveria trinervia. Journal of Experimental Botany **2019 v.70 no.3**, pp. 995-1004.

Doust A. 2007. Architectural evolution and its implications for domestication in grasses. Annals of Botany **100**, 941-950.

Dwyer SA, Ghannoum O, Nicotra A, von Caemmerer S. 2007. High temperature acclimation of C_4 photosynthesis is linked to changes in photosynthetic biochemistry. Plant, Cell & Environment **30**, 53-66.

Ermakova M, Bellasio C, Fitzpatrick D, Furbank RT, Mamedov F, von Caemmerer S. 2021. Up-regulation of bundle sheath electron transport capacity under limiting light in C₄ Setaria viridis. bioRxiv, 2021.2002.2010.430537.

bioRxiv preprint doi: https://doi.org/10.1101/2021.03.13.435281; this version posted March 14, 2021. The copyright holder for this preprint (which was not certified by peer review) is the author/funder. All rights reserved. No reuse allowed without permission.

Ermakova M, Lopez-Calcagno PE, Raines CA, Furbank RT, von Caemmerer S. 2019. Overexpression of the Rieske FeS protein of the Cytochrome b6f complex increases C4 photosynthesis in Setaria viridis. Communications Biology **2**, 314.
Evans JR. 1987. The dependence of quantum yield on wavelength and growth irradiance. Australian Journal of Plant Physiology **14**, 69-79.
Evans JR. 1989. Photosynthesis and nitrogen relationships in leaves of C_3 plants. Oecologia **78**, 9-19.
Evans JR, von Caemmerer S. 1996. Carbon Dioxide Diffusion inside Leaves. Plant Physiology **110**, 339-346.
Farquhar GD. 1983. On the nature of carbon isotope discrimination in C_4 species. Australian Journal of Plant Physiology **10**, 205-226.
Farquhar GD, von Caemmerer S. 1982. Modelling of photosynthetic response to environmental conditions. In: Lange OL, Nobel PS, Osmond CB, Ziegler H, eds. *Physiological Plant Ecology II. Encyclopedia of Plant Physiology, New Series, Vol. 12 B*, Vol. 12 B. Berlin Heidelberg: Springer Verlag, 550-587.
Farquhar GD, von Caemmerer S, Berry JA. 1980. A biochemical-model of photosynthetic CO_2 assimilation in leaves of C_3 species. Planta **149**, 78-90.
Furbank RT. 2011. Evolution of the C4 photosynthetic mechanism: are there really three C4 acid decarboxylation types? Journal of Experimental Botany **62**, 3103-3108.
Furbank RT, Chitty JA, Taylor WC. 2001. Transgenic Flaveria bidentis. Biotechnology in Agriculture and Forestry 48 : Transgenic Crops Iii **48**, 319-336.
Furbank RT, Chitty JA, von Caemmerer S, Jenkins CLD. 1996. Antisense RNA inhibition of *RbcS* gene expression reduces rubisco level and photosynthesis in the C_4 plant *Flaveria bidentis*. Plant Physiology **111**, 725-734.
Furbank RT, Jenkins CLD, Hatch MD. 1990. C_4 photosynthesis: quantum requirement, C_4 acid overcycling and *Q*-cycle involvement. Australian Journal of Plant Physiology **17**, 1-7.
Ghannoum O, Evans JR, Chow WS, Andrews TJ, Conroy JP, von Caemmerer S. 2005. Faster rubisco is the key to superior nitrogen-use efficiency in NADP-malic enzyme relative to NAD-malic enzyme C_4 grasses. Plant Physiology **137**, 638-650.
Gillon JS, Yakir D. 2000. Internal conductance to CO_2 diffusion and $C^{18}OO$ discrimination in C_3 leaves. Plant Physiology **123**, 201-213.
Harrison EP, Olcer H, Lloyd JC, Long SP, Raines CA. 2001. Small decreases in SBPase cause a linear decline in the apparent RuBP regeneration rate, but do not affect Rubisco carboxylation capacity. Journal of Experimental Botany **52**, 1779-1784.
Harrison EP, Willingham NM, Lloyd JC, Raines CA. 1998. Reduced sedoheptulose-1,7-bisphosphatase levels in transgenic tobacco lead to decreased photosynthetic capacity and altered carbohydrate accumulation. Planta **204**, 27-36.
Hatch MD. 1987. C_4 photosynthesis: A unique blend of modified biochemistry, anatomy and ultrastructure. Biochim.Biophys.Acta **895**, 81-106.
Hatch MD, Burnell JN. 1990. Carbonic anhydrase activity in leaves and its role in the first step of C_4 photosynthesis. Plant Physiology **93**, 825-828.
Hatch MD, Osmond CB. 1976. Compartmentation and transport in C_4 photosynthesis. In: Stocking CR, Heber U, eds. *Transport in plants 111*, Vol. 3. Berlin: Springer-Verlag.
Henderson S, von Caemmerer S, Farquhar GD. 1992. Short-term measurements of carbon isotope discrimination in several C_4 species. Australian Journal of Plant Physiology **19**, 263-285.
Jenkins CLD. 1989. Effects of the phosphoenolpyruvate carboxylase inhibitor 3,3-dichloro-2-(dihydroxyphosphinoylmethyl) propenoate on photosynthesis. C_4 selectivity and studies on C_4 photosynthesis. Plant Physiology **89**, 1231-1237.
Jenkins CLD, Furbank RT, Hatch MD. 1989. Inorganic carbon diffusion between C_4 mesophyll and bundle sheath cells. Direct bundle sheath CO_2 assimilation in intact leaves in the presence of an inhibitor of the C_4 pathway. Plant Physiology **91**, 1356-1363.

bioRxiv preprint doi: https://doi.org/10.1101/2021.03.13.435281; this version posted March 14, 2021. The copyright holder for this preprint (which was not certified by peer review) is the author/funder. All rights reserved. No reuse allowed without permission.

Jordan DB, Ogren WL. 1981. Species variation in the specificity of ribulose bisphosphate carboxylase/oxygenase. Nature **291**, 513-515.
Jordan DB, Ogren WL. 1983. Species variation in kinetic-properties of ribulose 1,5-bisphosphate carboxylase oxygenase. Archives of Biochemistry and Biophysics **227**, 425-433.
Jordan DB, Ogren WL. 1984. The CO2/O2 specificity of ribulose 1,5-bisphosphate carboxylase oxygenase - dependence on ribulosebisphosphate concentration, PH and temperature. Planta **161**, 308-313.
June T, Evans JR, Farquhar GD. 2004. A simple new equation for the reversible temperature dependence of photosynthetic electron transport: a study on soybean leaf. Functional Plant Biology **31**, 275-283.
King JL, Edwards GE, Cousins AB. 2012. The efficiency of the CO_2-concentrating mechanism during single-cell C_4 photosynthesis. Plant Cell and Environment **35**, 513-523.
Krall JP, Pearcy RW. 1993. Concurrent measurements of oxygen and carbon dioxide exchange during lightflecks in maize (zea mays l). Plant Physiology **103**, 823-828.
Kromdijk J, Griffiths H, Schepers HE. 2010. Can the progressive increase of C_4 bundle sheath leakiness at low PFD be explained by incomplete suppression of photorespiration? Plant Cell and Environment **33**, 1935-1948.
Kubásek J, Urban O, Šantrůček J. 2013. C4 plants use fluctuating light less efficiently than do C3 plants: a study of growth, photosynthesis and carbon isotope discrimination. Physiologia Plantarum **149**, 528-539.
Kubien DS, von Cammerer S, Furbank RT, Sage RF. 2003. C_4 photosynthesis at low temperature. A study using transgenic plants with reduced amounts of Rubisco. Plant Physiology **132**, 1577-1585.
Leakey ADB, Uribelarrea M, Ainsworth EA, Naidu SL, Rogers A, Ort DR, Long SP. 2006. Photosynthesis, productivity, and yield of maize are not affected by open-air elevation of CO2 concentration in the absence of drought. Plant Physiology **140**, 779-790.
Leegood RC, von Caemmerer S. 1988. The relationship between contents of photosynthetic metabolites and the rate of photosynthetic carbon assimilation in the leaves of *Amaranthus edulis* L. Planta **174**, 253-265.
Leegood RC, von Caemmerer S. 1989. Some relationships between contents of photosynthetic intermediates and the rate of photosynthetic carbon assimilation in leaves of *Zea mays* L. Planta **178**, 258-266.
Li PH, Brutnell TP. 2011. Setaria viridis and Setaria italica, model genetic systems for the Panicoid grasses. Journal of Experimental Botany **62**, 3031-3037.
Long SP. 1999. Environmental responses. In: Sage RF, Monson R, eds. *C4 Plant Biology*. San Diego: Academic Press, 215-250.
Long S P, Marshall-Colon A, Zhu X. 2015. Meeting the Global Food Demand of the Future by Engineering Crop Photosynthesis and Yield Potential. Cell **161**, 56-66.
Ludwig M, von Caemmerer S, Price GD, Badger MR, Furbank RT. 1998. Expression of tobacco carbonic anhydrase in the C_4 dicot *Flaveria bidentis* leads to increased leakiness of the bundle sheath and a defective CO_2-concentrating mechanism. Plant Physiology **117**, 1071-1081.
Massad RS, Tuzet A, Bethenod O. 2007. The effect of temperature on C_4-type leaf photosynthesis parameters. Plant Cell and Environment **30**, 1191-1204.
Meinzer FC, Zhu J. 1998. Nitrogen stress reduces the efficiency of the c-4 co2 concentrating system, and therefore quantum yield, in saccharum (sugarcane) species. Journal of Experimental Botany **49**, 1227-1234.
Mitchell PL, Sheehy JE. 2006. Supercharging rice photosynthesis to increase yield. New Phytologist **171**, 688-693.
Ogée J, Wingate L, Genty B. 2018. Estimating mesophyll conductance from measurements of $C^{18}OO$ discrimination and carbonic anhydrase activity. Plant Physiology **178**, 728-752.
Ogren E, Evans JR. 1993. Photosynthethic light response curves. I. the influence of CO_2 partial pressure and leaf inversion. Planta **189**, 182-190.

bioRxiv preprint doi: https://doi.org/10.1101/2021.03.13.435281; this version posted March 14, 2021. The copyright holder for this preprint (which was not certified by peer review) is the author/funder. All rights reserved. No reuse allowed without permission.

Osborn HL, Alonso-Cantabrana H, Sharwood RE, Covshoff S, Evans JR, Furbank RT, von Caemmerer S. 2016. Effects of reduced carbonic anhydrase activity on CO_2 assimilation rates in *Setaria viridis*: a transgenic analysis. Journal of Experimental Botany, erw357.

Peisker M. 1979. Conditions of low, and oxygen-independent, CO_2 compensation concentrations in C_4 plants as derived from a simple model. Photosynthetica **13**, 198-207.

Peisker M. 1986. Models of carbon metabolism in C_3-C_4 intermediate plants as applied to the evolution of C_4 photosynthesis. Plant, Cell and Environment **9**, 627-635.

Peisker M. 1988. Modelling of C_4 photosynthesis at low quantum flux densities. In: Valnikov S, Stanev D, Dilova M, eds. *International Symposium on Plant Mineral Nutrition and Photosynthesis*, Vol. II. Sofia: Bulgarian Academy of Science, 226-234.

Peisker M, Henderson SA. 1992. Carbon - Terrestrial C_4 Plants. Plant Cell and Environment **15**, 987-1004.

Pengelly JJL, Sirault XRR, Tazoe Y, Evans JR, Furbank RT, von Caemmerer S. 2010. Growth of the C_4 dicot *Flaveria bidentis*: photosynthetic acclimation to low light through shifts in leaf anatomy and biochemistry. Journal of Experimental Botany **61**, 4109-4122.

Pengelly JJL, Tan J, Furbank RT, von Caemmerer S. 2012. Antisense reduction of NADP-malic enzyme in *Flaveria bidentis* reduces flow of CO_2 through the C_4 Cycle. Plant Physiology **160**, 1070-1080.

Petersen J, Förster K, Turina P, Gräber P. 2012. Comparison of the H^+/ATP ratios of the H^+-ATP synthases from yeast and from chloroplast. Proceedings of the National Academy of Sciences **109**, 11150-11155.

Pfeffer M, Peisker M. 1998. CO_2 gas exchange and phosphoenolpyruvate carboxylase activity in leaves of *Zea mays* L. Photosynthesis Research **58**, 281-291.

Pfundel E, Pfeffer M. 1997. Modification of photosystem i light harvesting of bundle-sheath chloroplasts occurred during the evolution of nadp-malic enzyme c-4 photosynthesis. Plant Physiology **114**, 145-152.

Price GD, Badger MR, von Caemmerer S. 2011. The prospect of using cyanobacterial bicarbonate transporters to improve leaf photosynthesis in C_3 crop plants. Plant Physiology **155**, 20-26.

Raven JA. 1977. Ribulose bisphosphate carboxylase activity in terrestrial plants: significance of O_2 and CO_2 diffusion. Current Advances in Plant Science **9**, 579-590.

Rogers A, Medlyn BE, Dukes JS, Bonan G, von Caemmerer S, Dietze MC, Kattge J, Leakey ADB, Mercado LM, Niinemets Ü, Prentice IC, Serbin SP, Sitch S, Way DA, Zaehle S. 2017. A roadmap for improving the representation of photosynthesis in Earth system models. New Phytologist **213**, 22-42.

Sage RF, Pearcy RW. 1987. The nitrogen use efficiency of C3 and C4 plants. II Leaf nitrogen effects on the gas exchange characterisitcs of *Chenopodium album* L. and *Amaranthus retroflexus* L. Plant Physiology **84**, 959-963.

Salesse-Smith CE, Sharwood RE, Busch FA, Kromdijk J, Bardal V, Stern DB. 2018. Overexpression of Rubisco subunits with RAF1 increases Rubisco content in maize. Nature Plants **4**, 802-810.

Sharkey TD, Bernacchi CJ, Farquhar GD, Singsaas EL. 2007. Fitting photosynthetic carbon dioxide response curves for C_3 leaves. Plant Cell and Environment **30**, 1035-1040.

Sharwood RE, Ghannoum O, Kapralov MV, Gunn LH, Whitney SM. 2016. Temperature responses of Rubisco from Paniceae grasses provide opportunities for improving C_3 photosynthesis. Nature Plants **2**, 16186.

Siebke K, Voncaemmerer S, Badger M, Furbank RT. 1997. Expressing an rbcs antisense gene in transgenic *Flaveria bidentis* leads to an increased quantum requirement for CO_2 fixed in photosystems I and II. Plant Physiology **115**, 1163-1174.

Sonawane BV, Sharwood RE, von Caemmerer S, Whitney SM, Ghannoum O. 2017. Short-term thermal photosynthetic responses of C4 grasses are independent of the biochemical subtype. Journal of Experimental Botany **68**, 5583-5597.

Studer AJ, Gandin A, Kolbe AR, Wang L, Cousins AB, Brutnell TP. 2014. A limited role for carbonic anhydrase in C_4 photosynthesis as revealed by a ca1ca2 double mutant in maize. Plant Physiology **165**, 608-617.

bioRxiv preprint doi: https://doi.org/10.1101/2021.03.13.435281; this version posted March 14, 2021. The copyright holder for this preprint (which was not certified by peer review) is the author/funder. All rights reserved. No reuse allowed without permission.

Sun W, Ubierna N, Ma JY, Cousins AB. 2012. The influence of light quality on C_4 photosynthesis under steady-state conditions in Zea mays and Miscanthus giganteus: changes in rates of photosynthesis but not the efficiency of the CO_2 concentrating mechanism. Plant Cell and Environment **35**, 982-993.

Trevanion SJ, Furbank RT, Ashton AR. 1997. Nadp-malate dehydrogenase in the c-4 plant flaveria bidentis - cosense suppression of activity in mesophyll and bundle-sheath cells and consequences for photosynthesis. Plant Physiology **113**, 1153-1165.

Ubierna N, Gandin A, Boyd RA, Cousins AB. 2016. Temperature response of mesophyll conductance in three C_4 species calculated with two methods: ^{18}O discrimination and in vitro Vpmax. New Phytologist **214** 66-80.

Ubierna N, Gandin A, Boyd RA, Cousins AB. 2017. Temperature response of mesophyll conductance in three C_4 species calculated with two methods: ^{18}O discrimination and in vitro V_{pmax}. New Phytologist **214**, 66-80.

Ubierna N, Sun W, Cousins AB. 2011. The efficiency of C_4 photosynthesis under low light conditions: assumptions and calculations with CO_2 isotope discrimination. Journal of Experimental Botany **62**, 3119-3134.

Ubierna N, Sun W, Kramer DM, Cousins AB. 2013. The efficiency of C_4 photosynthesis under low light conditions in *Zea mays*, *Miscanthus x giganteus* and *Flaveria bidentis*. Plant Cell and Environment **36**, 365-381.

Usuda H. 1984. Variations in the photosynthesis rate and activity of photosynthetic enzymes in maize leaf tissue of different ages. Plant and Cell Physiology **25**, 1297-1301.

Usuda H, Ku MSB, Edwards GE. 1984. Rates of photosynthesis relative to activity of photosynthetic enzymes, chlorophyll and soluble protein content among ten C_4 species. Australian Journal of Plant Physiology **11**, 509-517.

Vollmar M, Schlieper D, Winn M, Büchner C, Groth G. 2009. Structure of the C14-rotor ring of the proton translocating chloroplast ATP synthase. Journal of Biological Chemistry.

von Caemmerer S. 2000. *Biochemical models of leaf photosynthesis*. Collingwood, Australia: CSIRO Publishing.

von Caemmerer S, Evans JR. 1991. Determination of the average partial pressure of CO_2 in chloroplast from leaves of several C_3 plants. Australian Journal Plant Physiology **18**, 287-305.

von Caemmerer S, Evans JR. 2010. Enhancing C_3 photosynthesis. Plant Physiology **154**, 589-592.

von Caemmerer S, Farquhar GD. 1981. Some relationships between the biochemistry of photosynthesis and the gas exchange of leaves. Planta **153**, 376-387.

von Caemmerer S, Furbank RT. 1999. Modeling of C_4 photosynthesis. In: Sage RF, Monson R, eds. *C_4 plant biology*. San Diego, CA, USA: Academic Press, 169-207.

von Caemmerer S, Furbank RT. 2003. The C_4 pathway: an efficient CO_2 pump. Photosynthesis Research **77**, 191-207.

von Caemmerer S, Furbank RT. 2016. Strategies for improving C 4 photosynthesis. Current Opinion in Plant Biology **31**, 125-134.

von Caemmerer S, Millgate A, Farquhar GD, Furbank RT. 1997. Reduction of ribulose-1,5-bisphosphate carboxylase/oxygenase by antisense RNA in the C_4 plant *Flaveria bidentis* leads to reduced assimilation rates and increased carbon isotope discrimination. Plant Physiology **113**, 469-477.

von Caemmerer S, Quinn V, Hancock NC, Price GD, Furbank RT, Ludwig M. 2004. Carbonic anhydrase and C_4 photosynthesis: a transgenic analysis. Plant, Cell & Environment **27**, 697-703.

von Caemmerer S, Susanne, caemmerer@anu, edu, au. 2003. C_4 photosynthesis in a single C_3 cell is theoretically inefficient but may ameliorate internal CO_2 diffusion limitations of C_3 leaves. Plant, Cell & Environment **26**, 1191-1197.

Wong SC, Cowan IR, Farquhar GD. 1985. Leaf conductance in relation to rate of CO_2 assimilation. I Influence of nitrogen nutrition, phosphorus nutrition, photon flux densitiy, and ambient partial pressure of CO2 during ontogeny. Plant Physiology **78**, 821-825.

bioRxiv preprint doi: https://doi.org/10.1101/2021.03.13.435281; this version posted March 14, 2021. The copyright holder for this preprint (which was not certified by peer review) is the author/funder. All rights reserved. No reuse allowed without permission.

Wu A, Doherty A, Farquhar GD, Hammer GL. 2018. Simulating daily field crop canopy photosynthesis: an integrated software package. Functional Plant Biology **45**, 362-377.
Wu A, Hammer GL, Doherty A, von Caemmerer S, Farquhar GD. 2019. Quantifying impacts of enhancing photosynthesis on crop yield. Nature Plants **5**, 380-388.
Yamori W, Evans JR, von Caemmerer S. 2010. Effects of growth and measurement light intensities on temperature dependence of CO_2 assimilation rate in tobacco leaves. Plant Cell and Environment **33**, 332-343.
Yin X, Struik PC. 2009. C_3 and C_4 photosynthesis models: An overview from the perspective of crop modelling. Njas-Wageningen Journal of Life Sciences **57**, 27-38.
Yin X, Van Oijen M, Schapendonk A. 2004. Extension of a biochemical model for the generalized stoichiometry of electron transport limited C_3 photosynthesis. Plant Cell and Environment **27**, 1211-1222.
Yin XY, Struik PC. 2012. Mathematical review of the energy transduction stoichiometries of C_4 leaf photosynthesis under limiting light. Plant Cell and Environment **35**, 1299-1312.
Yin XY, Sun ZP, Struik PC, Van der Putten PEL, Van Ieperen W, Harbinson J. 2011. Using a biochemical C4 photosynthesis model and combined gas exchange and chlorophyll fluorescence measurements to estimate bundle-sheath conductance of maize leaves differing in age and nitrogen content. Plant Cell and Environment **34**, 2183-2199.
Zhou H, Akcay E, Helliker B. 2017. Deriving C₄ photosynthesis parameters by fitting intensive A/C_i curves. bioRxiv.
Zhou H, Akçay E, Helliker BR. 2019. Estimating C_4 photosynthesis parameters by fitting intensive A/Ci curves. Photosynthesis Research.